MODELING FLYWHEEL-SPEED VARIATIONS BASED ON CYLINDER PRESSURE

Master's thesis
performed in **Vehicular Systems**

by
Magnus Nilsson

Reg nr: LiTH-ISY-EX-3584-2004

30th March 2004

MODELING FLYWHEEL-SPEED VARIATIONS BASED ON CYLINDER PRESSURE

Master's thesis

performed in **Vehicular Systems**,
Dept. of Electrical Engineering
at **Linköpings universitet**

by **Magnus Nilsson**

Reg nr: LiTH-ISY-EX-3584-2004

Supervisor: **Mats Järgenstedt**
Scania
Associate Professor Lars Eriksson
Linköpings Universitet

Examiner: **Associate Professor Lars Eriksson**
Linköpings Universitet

Linköping, 30th March 2004

Avdelning, Institution
Division, Department

Vehicular Systems,
Dept. of Electrical Engineering
581 83 Linköping

Datum
Date

30th March 2004

Språk
Language
☐ Svenska/Swedish
☒ Engelska/English
☐ ____________

Rapporttyp
Report category
☐ Licentiatavhandling
☒ Examensarbete
☐ C-uppsats
☐ D-uppsats
☐ Övrig rapport
☐ ____________

ISBN
—

ISRN
LITH-ISY-EX-3584-2004

Serietitel och serienummer
Title of series, numbering

ISSN
—

URL för elektronisk version

http://www.vehicular.isy.liu.se
http://www.ep.liu.se/exjobb/isy/2004/3584/

Titel ATT MODELLERA SVÄNGHJULSHASTIGHET BASERAT PÅ CYLINDERTRYCK

Title MODELING FLYWHEEL-SPEED VARIATIONS BASED ON CYLINDER PRESSURE

Författare Magnus Nilsson
Author

Sammanfattning
Abstract

Combustion supervision by evaluating flywheel speed variations is a common approach in the automotive industry. This often involves preliminary measurements. An adequate model for simulating flywheel speed can assist to avoid some of these preliminary measurements.

A physical nonlinear model for simulating flywheel speed based on cylinder pressure information is investigated in this work. Measurements were conducted at Scania in a test bed and on a chassis dynamometer. The model was implemented in MATLAB/Simulink and simulations are compared to measured data. The first model can not explain all dynamics for the measurements in the test bed so extended models are examined. A model using a dynamically equivalent model of the crank-slider mechanism shows no difference from the simple model, whereas a model including a driveline can explain more from the test-bed measurements. When simulating the setups used at the chassis dynamometer, the simplest model works best. Yet, it is not very accurate and it is proposed that optimization of parameter values might improve the model further. A sensitivity analysis shows that the model is fairly robust to parameter changes.

A continuation of this work might include optimization to estimate parameter values in the model. Investigating methods for combustion supervision may also be a future issue.

Nyckelord
Keywords
combustion supervision, cylinder balancing, physical model, cylinder pressure, flywheel speed, crankshaft

Abstract

Combustion supervision by evaluating flywheel speed variations is a common approach in the automotive industry. This often involves preliminary measurements. An adequate model for simulating flywheel speed can assist to avoid some of these preliminary measurements.

A physical nonlinear model for simulating flywheel speed based on cylinder pressure information is investigated in this work. Measurements were conducted at Scania in a test bed and on a chassis dynamometer. The model was implemented in MATLAB/Simulink and simulations are compared to measured data. The first model can not explain all dynamics for the measurements in the test bed so extended models are examined. A model using a dynamically equivalent model of the crank-slider mechanism shows no difference from the simple model, whereas a model including a driveline can explain more from the test-bed measurements. When simulating the setups used at the chassis dynamometer, the simplest model works best. Yet, it is not very accurate and it is proposed that optimization of parameter values might improve the model further. A sensitivity analysis shows that the model is fairly robust to parameter changes.

A continuation of this work might include optimization to estimate parameter values in the model. Investigating methods for combustion supervision may also be a future issue.

Keywords: combustion supervision, cylinder balancing, physical model, cylinder pressure, flywheel speed, crankshaft

Preface

This work constitutes a master's thesis at the Division of Vehicular Systems, Linköpings universitet. The work was carried out during september to november 2003 under the supervision of Mats Järgenstedt at Scania, Södertälje. From november 2003 to march 2004, the work was completed at Linköpings universitet under the supervision of Assoc. Prof. Lars Eriksson. It was financially supported by Scania which has been much acknowledged.

Thesis Outline

Chapter 1 gives an introduction to the problem and outlines the objectives of this thesis.
Chapter 2 summarizes the model described in [14].
Chapter 3 describes measurements carried out at Scania.
Chapter 4 discusses results from simulations for various models.
Chapter 5 sums up conclusions from the present work.
Chapter 6 discusses future work.
Appendix A contains information related to the derivation of extended models.

Acknowledgment

I would like to thank my supervisors, Assoc. Prof. Lars Eriksson at the Division of Vehicular Systems, Linköpings universitet, and Mats Järgenstedt at Scania. Lars gave me the oppurtunity to work with this problem and contributed with well-needed advise. Mats took care of me at Scania and gave me a good introduction to the problem and the major outline of my assignment. I am also grateful for the assistance given at the measurements in the test-bed environment and at the chassis dynamometer. I would further like to thank Mats Henriksson for introducing me to Rotec and Henrik Pettersson for assistance at the chassis dynamometer. General appreciation is directed to all people at Scania that assisted me during my stay in Södertälje. A special thanks to people at NEE, Scania, and the Division of Vehicular Systems, Linköping, for giving up time to answer questions related to my work. Finally, much thanks to my family for your constant love and support.

Contents

Abstract v

Preface and Acknowledgment vii

1 Introduction 1
- 1.1 Combustion Supervision 1
- 1.2 Objectives 2

2 The Model 3
- 2.1 Torque due to Cylinder Pressure 3
- 2.2 Torque due to Motion of Masses 4
- 2.3 The Torque-Balancing Equation 5
- 2.4 Crankshaft Dynamics 5
- 2.5 A Time-Domain State-Space Model 8

3 Measurements 9
- 3.1 Planning the Measurements—Things to Consider 9
  - 3.1.1 Measuring Cylinder Pressure 9
  - 3.1.2 Measuring Flywheel Speed 9
  - 3.1.3 The Importance of a High Sample Rate 10
- 3.2 Using Indiscope 11
- 3.3 Using Rotec 13
  - 3.3.1 Measuring Cylinder Pressure With Rotec 14
  - 3.3.2 Transforming Domains for Measured Signals . . 14
  - 3.3.3 A Short Analysis of the Constructed Signals . . . 18
  - 3.3.4 Reason for the Noisy Speed Signal 18
  - 3.3.5 Speed Comparison—S6 and Rotec 19
- 3.4 The Chassis Dynamometer 21
  - 3.4.1 Speed Comparison—MIKE and MOA 22
  - 3.4.2 Speed Comparison—Trucks and Rotec 22

4 Simulations **27**
4.1 The Simple Model 28
4.2 A Dynamically Equivalent Model 31
4.3 Including a Model of the Driveline 32
4.4 A Truck-Driveline Model 35
4.4.1 Speed Comparison—Simple- and Driveline Model 35
4.4.2 Speed Comparison—Driveline Model and Rotec . 38
4.5 Trial-and-Error Modeling 40
4.5.1 An Alternative Damper Model 40
4.5.2 Manipulating Stiffness Parameters 40
4.6 Sensitivity Analysis 44

5 Conclusions **51**
5.1 Conclusions from the Measurements 51
5.2 Conclusions from the Simulations 52

6 Future Work **53**

References **55**

A Equations for Extended Models **57**
A.1 A Dynamically Equivalent Model of the Connecting Rod 57
A.2 A Simple Truck-Driveline Model 59

List of Tables

3.1 Operating Points—First Measurement 12
3.2 Operating Points—Second Measurement 14
3.3 Operating Points—Third Measurement 21

List of Figures

2.1 The Crank-Slider Mechanism 4
2.2 The Lumped Mass Model 6

3.1 Circular Disc and Flywheel 10
3.2 Schematic Engine Setup in Test Beds 11
3.3 Indiscope Speed Signal 12
3.4 Measured Signals with Rotec 13
3.5 Adjusting the Measured Pressure Curve 15
3.6 Cancellation Phenomenon in the Speed Signal 16
3.7 Transforming Domain for the Pressure Signal 17
3.8 Cycle-to-Cycle Variations in Pressure 18
3.9 Noisy Speed Signal From Rotec 19
3.10 Speed Comparison—S6 and Rotec, 1500 rpm 20
3.11 Chassis Dynamometer Setup 21
3.12 Speed Comparison—MIKE and MOA, 1500 rpm 22
3.13 Speed Comparison—MIKE and MOA, 1000 rpm 23
3.14 Speed Comparison—MIKE and Rotec, 1500 rpm 24
3.15 Speed Comparison—MOA and Rotec, 1900 rpm 25

4.1 Simulation—Simple Model, 1000 rpm 28
4.2 Simulation—Simple Model, 1500 rpm 29
4.3 Simulation—Simple Model, 1900 rpm 30
4.4 Comparison—Simple- and DE Model, 1900 rpm 31
4.5 The Lumped Mass Model Including a Driveline 32
4.6 Transient Response when a Driveline is Included 33
4.7 Simulation—Test Bed Driveline, 1500 rpm 33
4.8 Simulation—Test Bed Driveline, Offset Engine 34
4.9 Comparison—Simple- and MALTE Model, 1000 rpm . . 36
4.10 Comparison—Simple- and MALTE Model, 1900 rpm . . 37
4.11 Simulation—MALTE Model, 1000 rpm 38
4.12 Simulation—MALTE Model, 1900 rpm 39
4.13 Simulation—Alternative Damper Model 41
4.14 Simulation—Modified Stiffness 42
4.15 Sensitivity Analysis, Offset Pressure 44

4.16 Sensitivity Analysis, Scaled Pressure 45
4.17 Sensitivity Analysis, Translated Pressure 46
4.18 Sensitivity Analysis, Stiffness Parameters 47
4.19 Sensitivity Analysis, Inertias 48

A.1 The Crank-Slider Mechanism 58
A.2 A Vehicular Driveline 59
A.3 Free-Body Diagram of a Driveline 59

Chapter 1

Introduction

1.1 Combustion Supervision

The electronic control system which covers at least the functioning of the fuel injection and ignition is called the Engine Management System. One objective for the system is to supervise cylinder combustion in order to avoid undesirable vibrations in parts of the engine. Undesirable vibrations in the crankshaft can arise from defective fuel injectors. There have been many articles and books written on how to discover control this phenomenon [5, 6, 9, 15].

A common approach on combustion supervision and cylinder balancing demands properties of the transfer function from cylinder pressures to flywheel speed. Thus, the method involves preliminary measurements on the engine.

A general physical model that can simulate flywheel speed using cylinder pressure as input can facilitate to gain more information on the transfer function. The focus of this thesis has been to implement and examine the properties of one such physical model.

1.2 Objectives

The general objectives were to

- Implement a basic mathematical model in Simulink that can simulate flywheel speed, given cylinder pressures.
- Carry out measurements that hold enough data to test and verify the mathematical model.

If those objectives were met, the next step would be to

- Compare the basic mathematical model with some extended models with a focus on examining torque contributions from drivelines.

or

- Investigate algorithms for cylinder pressure supervision.

The first two objectives were reached, although it was hard to judge the validity of the model. Then, comparisons with other models were made with an emphasis on driveline models. No time was spent on investigating cylinder pressure supervision.

Much work was spent on programming and a “toolbox” evolved as a corollary of working with the models in Matlab. See [12] for more details.

Chapter 2

The Model

This chapter summarizes the model developed by Schagerberg and McKelvey [14], and it follows their presentation to a high degree. The chapter may be skipped if familiar to the reader.

The model is a physical nonlinear lumped mass model which comprises the damper, the crankshaft, the cylinders and the flywheel. Given pressures as a function of crank angle, an equation for the equivalent torque on the crankshaft may be set up, based on cylinder and crank-slider information. Together with a model of the crankshaft, a torque balance equation is used to obtain a differential equation that may be implemented in e.g. Simulink.

2.1 Torque due to Cylinder Pressure

We define the differential *gas pressure*, $p_g(\theta)$, as the difference between the absolute pressure inside the combustion chamber and the counteracting pressure on the back side of the piston. When the gas pressure is multiplied by the piston area, A_p, we get the force that acts on the piston along the cylinder axis. The gas pressure is further transformed into the *gas torque*, $T_g(\theta)$, on the crankshaft by the crank-slider mechanism,

$$T_g(\theta) = p_g(\theta) A_p \frac{ds}{d\theta} \tag{2.1}$$

where θ denotes the *crank angle* and s denotes the *piston displacement*—see figure 2.1. The derivation of $\frac{ds}{d\theta}$ may be found in e.g. [9].

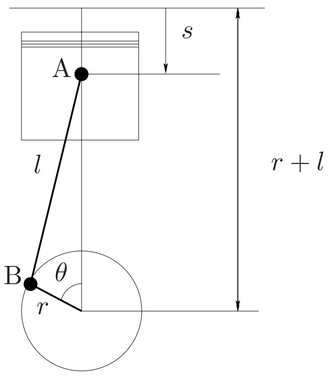

Figure 2.1: *The crank-slider mechanism.*

2.2 Torque due to Motion of Crank-Slider Mechanism Masses

The moment of inertia is a function of both mass and position. In the case of a crank-slider mechanism where the geometry changes, the moment of inertia will also vary. The term *varying inertia* will be used for this effect. The piston motion is assumed to be purely translational along the cylinder axis, why it dynamically can be described by a single point mass along this axis. Describing the motion of the crank-slider mechanism is more complex since it undertakes both translational and rotational motion. For a *dynamically equivalent model* of the connecting rod, three requirements must be satisfied:

1. The total mass of the model must be equal to that of the original body.

2. The center of gravity must be the same as for the original body.

3. The moment of inertia must be equal to that of the original body.

A common approximation is to consider a *statically equivalent model* in which the last requirement is not fulfilled. A statically equivalent model is used in most of this work. Thus, the piston and connecting rod are approximated by two point masses—one reciprocating, m_A, and one rotating, m_B—placed at the centers of the piston pin and crank pin respectively as in figure 2.1. A dynamically equivalent model is briefly examined in section 4.2.

The mass torque may be derived in different ways. In [9] it is done considering the kinetic energy of the two point masses, m_A and m_B.

The resulting equation may be expressed as

$$T_m(\theta,\dot{\theta},\ddot{\theta}) = -(J_A(\theta)+m_B r^2)\ddot{\theta} - \frac{1}{2}\frac{dJ_A(\theta)}{d\theta}\dot{\theta}^2, \tag{2.2}$$

where the varying inertia of m_A with respect to the crankshaft axis, $J_A(\theta)$, and its derivative with respect to θ are

$$J_A(\theta) = m_A\left(\frac{ds}{d\theta}\right)^2 \tag{2.3}$$

$$\frac{dJ_A(\theta)}{d\theta} = 2m_A\frac{d^2s}{d\theta^2}\frac{ds}{d\theta} \quad . \tag{2.4}$$

The expressions for the piston displacement may be found in [9].

2.3 The Torque-Balancing Equation

Summing up the torque contribution from a single cylinder gives a scalar differential equation, often referred to as the torque-balancing equation

$$J\ddot{\theta} = T_g(\theta) + T_m(\theta,\dot{\theta},\ddot{\theta}) + T_f(\theta) + T_l(\theta), \tag{2.5}$$

where J is the crankshaft inertia, $T_f(\theta)$ the friction torque and $T_l(\theta)$ the load torque. The mass torque, $T_m(\theta,\dot{\theta},\ddot{\theta})$ is given in equation (2.2).

The instantaneous friction torque, $T_f(\theta)$, is modeled as viscous dampers. Other torques that contribute to the crankshaft torque, such as the driving of auxiliary systems of the engine, are neglected in the model.

2.4 Crankshaft Dynamics

The main reason for using a lumped mass model of the crankshaft as the physical model in this work, is because such models are developed as standard procedure in the design phase of the crankshafts. The objective is then however to calculate the maximum torsional stresses in the shaft to mitigate crankshaft failure and for Noise Vibration and Harshness issues.

A multi-body extension of the torque-balancing equation (2.5) may be expressed as

$$\boldsymbol{J}\ddot{\boldsymbol{\theta}} + \boldsymbol{C}\dot{\boldsymbol{\theta}} + \boldsymbol{K}\boldsymbol{\theta} = \boldsymbol{T}_g(\boldsymbol{\theta}) + \boldsymbol{T}_m(\boldsymbol{\theta}) + \boldsymbol{T}_f(\boldsymbol{\theta}) + \boldsymbol{T}_l(\boldsymbol{\theta}), \tag{2.6}$$

where $\boldsymbol{\theta}$ is now a vector. In equation (2.6), $\boldsymbol{J}$, $\boldsymbol{K}$ and $\boldsymbol{C}$ are symmetric matrices and referred to as the inertia-, stiffness- and damping matrices respectively. These matrices are all of size $N \times N$, where N is the number of lumped masses. The damping elements are modeled as *viscous* *damping.* Stiffness and damping elements interconnected between adjacent lumped masses are here referred to as *relative*, and if connected between an inertia lump and a non-rotating reference *absolute.* For modeling of an engine crankshaft, typically both absolute and relative damping elements are used but only relative stiffness elements since the crankshaft is free to rotate about its axis.

In figure 2.2, such a model for the engine is outlined. Each relative

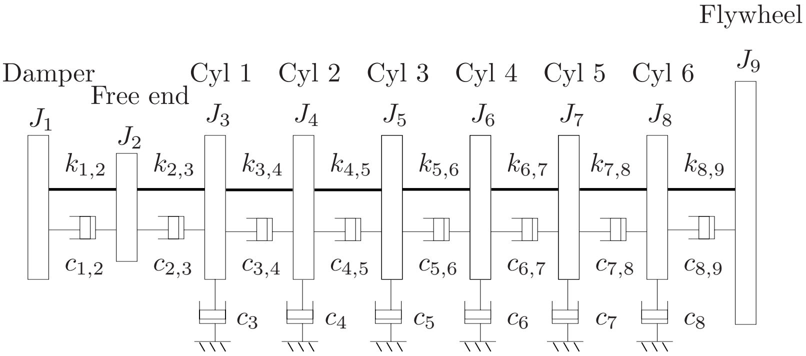

Figure 2.2: *The lumped mass model with interconnected stiffnesses and damping. Also absolute damping is included.*

stiffness- or damping element adds a 2×2 block matrix in the diagonal of $\boldsymbol{K}$ and $\boldsymbol{C}$ respectively. The block has the stiffness- or damping coefficient on the diagonal and the negative stiffness- of damping coefficient on the anti-diagonal. The load torque is assumed to be constant with respect to the time scale considered in this work. It is also assumed to be applied on the last mass in the crankshaft model. This simplifies the load torque into the constant vector,

$$\boldsymbol{T}_l = (0 \quad 0 \ \dots \ 0 \quad T_l)^T. \tag{2.7}$$

Friction torque is only modeled as viscous absolute damping elements. It is incorporated in the damping matrix $\boldsymbol{C}$ and consequently $\boldsymbol{T}_f(\boldsymbol{\theta}) = \boldsymbol{0}$.

To describe the cylinder positions in the model, define the *selection matrix* $\boldsymbol{S}$ of size $N \times N_c$, where N is the number of masses in the crankshaft model and N_c is the number of cylinders in the engine. The matrix $\boldsymbol{S}$ has ones in positions (n_{mass}, n_{cyl}), for $n_{cyl} = 1, \dots, N_c$. For a six-cylinder engine with cylinders in positions 3–8 in a nine-mass model,

$\boldsymbol{S}$ becomes

$$\boldsymbol{S} = (\boldsymbol{s}_1 \quad \dots \quad \boldsymbol{s}_{N_c}) = \begin{pmatrix} 0 & 0 & 0 & 0 & 0 & 0 \\ 0 & 0 & 0 & 0 & 0 & 0 \\ 1 & 0 & 0 & 0 & 0 & 0 \\ 0 & 1 & 0 & 0 & 0 & 0 \\ 0 & 0 & 1 & 0 & 0 & 0 \\ 0 & 0 & 0 & 1 & 0 & 0 \\ 0 & 0 & 0 & 0 & 1 & 0 \\ 0 & 0 & 0 & 0 & 0 & 1 \\ 0 & 0 & 0 & 0 & 0 & 0 \end{pmatrix}, \tag{2.8}$$

where $\boldsymbol{s}_i$ denotes the i:th column of $\boldsymbol{S}$. To simplify notation, the expressions for the gas and mass torques of a single cylinder (equations (2.1) and (2.2)) are used to define the following three geometrical functions,

$$\begin{aligned} g_1(\theta) &= A_p \frac{ds}{d\theta} && (2.9) \\ g_2(\theta) &= \frac{1}{2} J_a'(\theta) = m_A \frac{d^2 s}{d\theta^2} \frac{ds}{d\theta} && (2.10) \\ g_3(\theta) &= J_A(\theta) = m_A \Big(\frac{ds}{d\theta} \Big)^2. && (2.11) \end{aligned}$$

In a multicylinder engine the cylinder events are phased by the difference in firing angle between the cylinders. For instance, in the six-cylinder engines examined in this work the firing sequence is 1–5–3–6–2–4 and the crankshaft turns 120° between each firing. Thus define the phasing vector as

$$\boldsymbol{\Psi} = (\psi_1 \quad \dots \quad \psi_{N_c})^T. \tag{2.12}$$

The angles of the cranks reflect this phasing. For the multicylinder case, the geometrical functions $g_i(\theta)$, $i = 1, 2, 3$ in (2.9–2.11) may be used to define diagonal matrix functions,

$$\boldsymbol{G}_i(\boldsymbol{S}^T\boldsymbol{\theta} - \boldsymbol{\Psi}) = \operatorname{diag}\big(g_i(\boldsymbol{s}_1^T\boldsymbol{\theta} - \psi_1), \dots, g_i(\boldsymbol{s}_{N_c}^T\boldsymbol{\theta} - \psi_{N_c})\big). \tag{2.13}$$

The gas torque in the multi-body model may now be written

$$\boldsymbol{T}_g(\boldsymbol{\theta}) = \boldsymbol{S}\boldsymbol{G}_1(\boldsymbol{S}^T\boldsymbol{\theta} - \boldsymbol{\Psi})\boldsymbol{p}_g(\boldsymbol{S}^T\boldsymbol{\theta}). \tag{2.14}$$

Here, $\boldsymbol{p}_g(\cdot)$ is an $N_c \times 1$ vector function of the individual gas pressures. See equation (2.1) for the definition of gas torque in the single cylinder case. The multi-body extension of the single-cylinder mass torque defined in equation (2.2) becomes

$$\begin{aligned} \boldsymbol{T}_m(\boldsymbol{\theta}, \dot{\boldsymbol{\theta}}, \ddot{\boldsymbol{\theta}}) &= -\big(\boldsymbol{S}\boldsymbol{G}_3(\boldsymbol{S}^T\boldsymbol{\theta} - \boldsymbol{\Psi})\boldsymbol{S}^T + m_B r^2 \boldsymbol{S}\boldsymbol{S}^T\big)\ddot{\boldsymbol{\theta}} \\ &\quad -\boldsymbol{S}\boldsymbol{G}_2(\boldsymbol{S}^T\boldsymbol{\theta} - \boldsymbol{\Psi})\boldsymbol{S}^T\dot{\boldsymbol{\theta}} \odot \dot{\boldsymbol{\theta}}, && (2.15) \end{aligned}$$

where the symbol $\odot$ means elementwise multiplication.

2.5 A Time-Domain State-Space Model

The system of N second-order differential equations in equation (2.6) may be transformed into a system of $2N$ first-order differential equations e.g. by defining the state vector consisting of angles and rotational speeds,

$$\boldsymbol{x} = (\boldsymbol{x}_1^T \quad \boldsymbol{x}_2^T)^T = \big(\boldsymbol{\theta}^T \quad \dot{\boldsymbol{\theta}}^T\big)^T. \tag{2.16}$$

For convenience, the state vector is partitioned in position states $\boldsymbol{x}_1$ and speed states $\boldsymbol{x}_2$.

Now, to get to the state-space description of the model, we split the mass torque $\boldsymbol{T}_m(\boldsymbol{\theta}, \dot{\boldsymbol{\theta}}, \ddot{\boldsymbol{\theta}})$—see equation (2.15)—in the two parts multiplying angular acceleration and speed squared respectively, and define

$$\begin{aligned} \boldsymbol{T}_{m,1}(\boldsymbol{\theta}, \ddot{\boldsymbol{\theta}}) &= -\big(\boldsymbol{S}\boldsymbol{G}_3(\boldsymbol{S}^T\boldsymbol{\theta} - \boldsymbol{\Psi})\boldsymbol{S}^T + m_B r^2 \boldsymbol{S}\boldsymbol{S}^T\big)\ddot{\boldsymbol{\theta}} &\quad (2.17)\\ \boldsymbol{T}_{m,2}(\boldsymbol{\theta}, \dot{\boldsymbol{\theta}}) &= -\boldsymbol{S}\boldsymbol{G}_2(\boldsymbol{S}^T\boldsymbol{\theta} - \boldsymbol{\Psi})\boldsymbol{S}^T\dot{\boldsymbol{\theta}} \odot \dot{\boldsymbol{\theta}}. &\quad (2.18) \end{aligned}$$

We also define the *varying inertia* by collecting parts multiplying angular acceleration in equation (2.6), which give

$$\boldsymbol{J}(\boldsymbol{\theta}) = \boldsymbol{J} + m_B r^2 \boldsymbol{S}\boldsymbol{S}^T + \boldsymbol{S}\boldsymbol{G}_3(\boldsymbol{S}^T\boldsymbol{\theta} - \boldsymbol{\Psi})\boldsymbol{S}^T. \tag{2.19}$$

The torque-balancing equation may now be reformulated as

$$\boldsymbol{J}(\boldsymbol{\theta})\ddot{\boldsymbol{\theta}} = -\boldsymbol{K}\boldsymbol{\theta} - \boldsymbol{C}\dot{\boldsymbol{\theta}} + \boldsymbol{T}_{m,2}(\boldsymbol{\theta}, \dot{\boldsymbol{\theta}}) + \boldsymbol{T}_g(\boldsymbol{\theta}) + \boldsymbol{T}_l. \tag{2.20}$$

Stacking the identity equation $\dot{\boldsymbol{\theta}} = \boldsymbol{I}\dot{\boldsymbol{\theta}}$ together with equation (2.20) premultiplied by $\big(\boldsymbol{J}(\boldsymbol{\theta})\big)^{-1}$, the dynamics equation of the state-space model becomes

$$\begin{aligned} \dot{\boldsymbol{x}} &= \begin{pmatrix} \boldsymbol{0} & \boldsymbol{I} \\ -\big(\boldsymbol{J}(\boldsymbol{x}_1)\big)^{-1}\boldsymbol{K} & -\big(\boldsymbol{J}(\boldsymbol{x}_1)\big)^{-1}\boldsymbol{C} \end{pmatrix} \begin{pmatrix} \boldsymbol{x}_1 \\ \boldsymbol{x}_2 \end{pmatrix} \\ &+ \begin{pmatrix} \boldsymbol{0} \\ -\big(\boldsymbol{J}(\boldsymbol{x}_1)\big)^{-1}\boldsymbol{S}\boldsymbol{G}_2(\boldsymbol{S}^T\boldsymbol{x}_1 - \boldsymbol{\Psi})\boldsymbol{S}^T\boldsymbol{x}_2 \odot \boldsymbol{x}_2 \end{pmatrix} \\ &+ \begin{pmatrix} \boldsymbol{0} \\ -\big(\boldsymbol{J}(\boldsymbol{x}_1)\big)^{-1}\big(\boldsymbol{S}\boldsymbol{G}_1(\boldsymbol{S}^T\boldsymbol{x}_1 - \boldsymbol{\Psi})\boldsymbol{p}_g(\boldsymbol{S}^T\boldsymbol{x}_1) + \boldsymbol{T}_l\big) \end{pmatrix}. \end{aligned} \tag{2.21}$$

Equation (2.21) is divided in three terms to visualize the different contributions. The first term represents the crankshaft dynamics, the second term the piston-crank inertia effects, and the last term the input signals. Equation (2.21) and variations of it are used for simulations in this work. See section A.1 for more details about variations of equation (2.21).

Chapter 3

Measurements

We want to examine if a driveline has to be included to correctly simulate flywheel speed. In order to investigate this, measurements were made on heavy trucks mounted on a chassis dynamometer. However, another series of measurements was first conducted in a test bed to acquire pressure curves with synchronized speed signals.

3.1 Planning the Measurements—Things to Consider

3.1.1 Measuring Cylinder Pressure

We want to use measured or simulated cylinder pressure curves as input data to our model. This assumes that cycle-to-cycle variations are small, which should hold well for diesel engines, or that the model is robust with respect to input data. This should be verified to as a large extent as possible.

3.1.2 Measuring Flywheel Speed

There are two ways to measure flywheel speed in the test-bed environment:

1. The flywheels in Scania's heavy trucks have 60 bores[1] equidistantly drilled in the rim. A built-in hardware is used to measure time differences between the holes as they pass a sensor. An array of time differences may be extracted, where the first element corresponds to the time difference between top dead center (TDC) for cylinder 1 and the hole 6° thereafter. From this time-stamp

---

[1] One hole is "virtual" to allow for TDC localization.

array, flywheel speed as a function of flywheel position may be calculated. The built-in hardware is called *S6* and samples at a rate of 5 MHz.

2. There is a circular disc attached to the flywheel in the test bed. This circular disc, which is depicted in figure 3.1, holds 720 markers, or "teeth" as we will call them. The test beds are setup such that a transistor-transistor-logic (TTL) pulse-train signal may be extracted where each pulse correspond to a passed tooth.[2] The disc also holds a trigger tooth that (when passed) can be used as a reference to keep track of what angle we are on.[3] In the same way as S6 does, we may create an array of time differences between adjacent teeth and thereafter calculate flywheel speed as a function of flywheel position.

In the test bed, speed from both the flywheel and the circular disc are measured. One thing that should be investigated is if there are dynamics to be considered between the two rotating wheels.

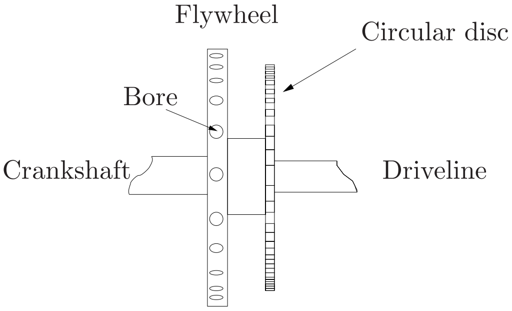

Figure 3.1: *A schematic view of the circular disc and flywheel in the test beds. Flywheel speed may be extracted from the built-in hardware (S6) and/or by measuring on the circular disc.*

3.1.3 The Importance of a High Sample Rate

We want to measure in-cycle speed variations which require a high sample rate on the TTL pulse-train signal extracted from the circular disc. How high can be roughly estimated using some simple calculations.

---

[2] This is not the whole truth. There is equipment in the test bed that extrapolates pulses to the TTL signal. This is discussed in section 3.3.4.

[3] Note that we can not be sure which phase in the cycle we are in when we pass the trigger tooth by only looking at the speed signal. The phase in the cycle is found out by also looking at a synchronized pressure curve.

Assume that we are running the engine at the true speed

$$\dot{\theta} = \frac{\Delta\theta}{\Delta t}\,, \tag{3.1}$$

that our circular disc has teeth with adjacent spacing $\Delta\theta$, and that we use the sample time T_s. Since the time samples may differ at most by T_s from the actual time that the sensor passes a tooth in the circular disc, the calculated speed of the circular disc based on two consecutive time stamps may be as high as $\Delta\theta/(\Delta t - T_s)$ or as low as $\Delta\theta/(\Delta t + T_s)$, depending on where the samples hit. We will denote the difference between these two values by the *speed uncertainty*, $\Delta\dot{\theta}$. The formula for speed uncertainty at speed $\dot{\theta}$ and angle resolution $\Delta\theta$ can be expressed as

$$\Delta\dot{\theta} = \frac{\Delta\theta}{\Delta t - T_s} - \frac{\Delta\theta}{\Delta t + T_s} = \frac{2\,\Delta\theta\,T_s\dot{\theta}^2}{(\Delta\theta)^2 - T_s^2\dot{\theta}^2}\,. \tag{3.2}$$

We want to keep $\Delta\dot{\theta}$ small, which requires a small value of T_s.

3.2 Test-Bed Measurements Using Indiscope

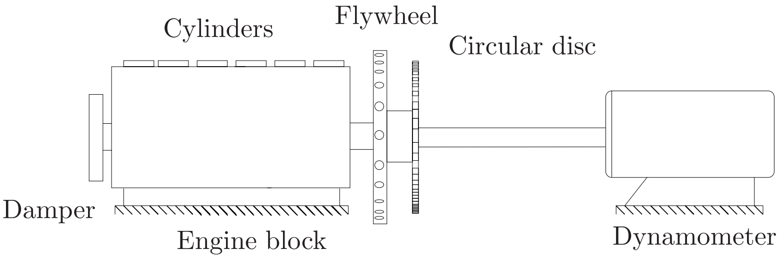

Figure 3.2: *Schematic engine setup in test beds.*

A D12 engine was mounted in a test bed. A schematic view of how the engines are mounted in test beds is shown in figure 3.2. The standard test bed equipment (Indiscope) was used to extract cylinder pressure and speed from the circular disc. Flywheel speed from S6 was not extracted. A map corresponding to table 3.1 was used for the measurements.

The importance of a high sample rate discussed in section 3.1.3 was overlooked. Indiscope samples at 500 kHz which gives a speed uncertainty $\Delta\dot{\theta} = 54$ rpm at 1500 rpm and $\Delta\theta = 1°$ using formula (3.2)—see also figure 3.3. Even a resampled signal with $\Delta\theta = 10°$ would still have a speed uncertainty of 5.4 rpm. This is not feasible for analysis or verification.

Load	1000 rpm	1500 rpm	1900 rpm
25%	*B*	*B*	*B*
50%	*B*	*B*,+1,±6	*B*
100%	*B*	*B*	*B*

Table 3.1: *Map of operating points used in the first series of measurements. A B means that the engine was kept balanced. A '+' followed by a number j, means that cylinder j was programmed to give a higher peak pressure than the rest of the cylinders. A '−' means that lower pressure was given by the cylinder compared to the others. The pressure was measured in cylinder 6.*

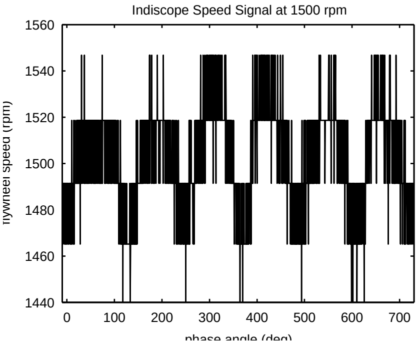

Figure 3.3: *The time stamps from Indiscope give a speed signal with low speed uncertainty. It can be seen in the figure that the speed resolution is approximately 54 rpm.*

3.3 Test-Bed Measurements Using Rotec

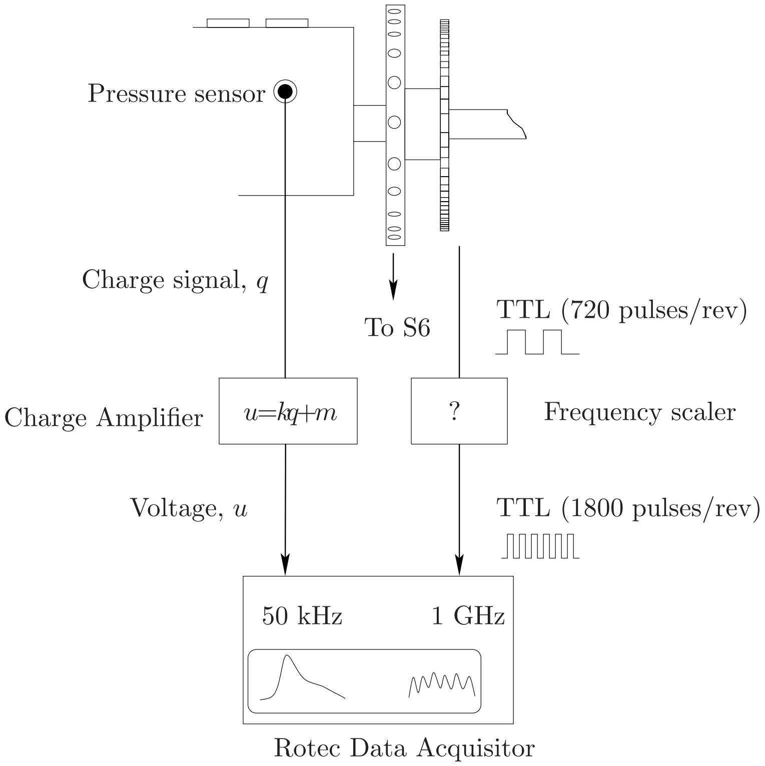
Pressure sensor
Charge signal, q
To S6
TTL (720 pulses/rev)
Charge Amplifier
u=kq+m
?
Frequency scaler
Voltage, u
TTL (1800 pulses/rev)
50 kHz
1 GHz
Rotec Data Acquisitor

Figure 3.4: *Signals measured with Rotec in the second series of measurements.*

Rotec RAS 5.0 is a data aquisition tool that can sample at a rate of up to 1 GHz for digital signals[4] (such as the speed signal) and 50 kHz for analogue signals (such as the pressure signal). It gives a speed uncertainty $\Delta\dot{\theta} = 0.027$ rpm at 1500 rpm and $\Delta\theta = 1°$.

Software was created for extracting flywheel speed data from S6. Using formula (3.2) we see that S6 with its six-degree spacing has a speed uncertainty $\Delta\dot{\theta} = 0.9$ rpm at 1500 rpm. Table 3.2 shows the map of operating points used in the second series of measurements.

---

[4] Rotec only saves time samples when it passes teeth (for digital signals) which means it uses small memory space as well.

Load	1000 rpm	1250 rpm	1500 rpm	1700 rpm	1900 rpm
100%	B	B	B,-5	B	B
50%	B	B	B,±5,±1,(+3-1)	B	B
25%	B	B	B	B	B
8%	B	B	B	B	B

Table 3.2: *Operating points used in the second series of measurements. The same notation as in table 3.1 is used. The parentheses indicate that more than one cylinder's pressure was altered in the same measurement. The pressure was measured in cylinder 5.*

3.3.1 Measuring Cylinder Pressure With Rotec

Signals with fast dynamics (apart from S6 data) were collected by Rotec to be able to synchronize pressure and speed signals.[5] The pressure sensor (from Kiestler) mounted on the cylinder is precise, and its signal value, $q = ap + b$, is approximately linear to cylinder pressure p. The signal q from the sensor is a charge which is transformed into a voltage, $u = kq + m$, through a linear charge amplifier—see figure 3.4. Thus, we have

$$u = kap + kb + m\,,$$

where the values of k and m are chosen such that the voltage ranges within the capability of Rotec's A/D converter. The linear constant k remains fixed once the charge amplifier is calibrated, while the constant m drifts slowly with time.

It was not feasible to recalibrate the charge amplifier once the measurements had started so it is assumed that the lowest pressure in the cylinder within a measurement is close to the exhaust pressure which is one of the measured mean-value signals. Using this signal, it is possible to offset the pressure curve to its (assumed) right position as shown in figure 3.5. Section 4.6 shows that the model output should not be significantly affected even if this would differ from the right lowest pressure by a few bars.

3.3.2 Transforming Domains for Measured Signals

All signals are measured in the time domain while the model uses the angular domain as a base for all signals. We therefore transform the measured signals onto the angular domain.

The only feasible way to get raw data from Rotec RAS 5.0 is to create DIA*dem* data sets and export them,[6] so a MATLAB function

---

[5] Additional interesting signals, such as torque load and exhaust pressure were mean value signals that could be collected from the measurement report, [3].

[6] The structure of DIA*dem* files can be found in e.g. [2].

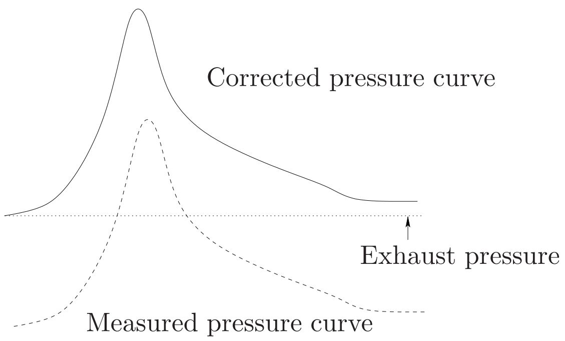

Figure 3.5: *Adjusting the measured pressure curve by offsetting it with the help of measured exhaust pressure.*

was created to parse simple DIA*dem* data files. Rotec hands over raw data in floating-point format. This results in cancellation when larger time-stamp values are used for calculating flywheel speed,[7] shown in figure 3.6. The interesting exported raw data are the time array $\boldsymbol{t} = (t_0 \ldots t_N)^T$ from the speed signal, the pressure array $\boldsymbol{p} = (p_0 \ldots p_M)^T$ and its corresponding time array $\boldsymbol{\tau} = (\tau_0 \ldots \tau_M)^T$.

Figure 3.7 depicts our method of transforming time- and pressure samples onto the angular domain. Assume that the first sample from the speed signal occurs at time t_0 and angle θ_0. If different spacing distances between teeth in the disc are neglected and Rotec's sample rate is considered as high, we can approximate a bijective discrete time function

$$\boldsymbol{t} = \boldsymbol{t}(\boldsymbol{\theta}) \iff \boldsymbol{\theta} = \boldsymbol{\theta}(\boldsymbol{t}), \tag{3.3}$$

where $\boldsymbol{\theta} = (\theta_0 + n\,\Delta\theta)_{n=1}^N$. The measured discrete pressure signal

$$\boldsymbol{p} = \boldsymbol{p}(\boldsymbol{\tau}) \tag{3.4}$$

is also a function of time where every time stamp from the pressure signal is wedged in between two time stamps from the speed signal. Consider an arbitrary time stamp τ_k from the pressure signal that is wedged in between two time stamps $t_j = t(\theta_j)$, and $t_{j+1} = t(\theta_{j+1})$ from the speed signal such that

$$\tau_k = (1 - \alpha)t_j + \alpha t_{j+1}, \quad \alpha \in [0\ 1]. \tag{3.5}$$

The distance $\Delta\theta$ between θ_j and θ_{j+1} is small so we use linear interpolation to define the bijective function

$$\boldsymbol{\vartheta} = \boldsymbol{\vartheta}(\boldsymbol{\tau}) \iff \boldsymbol{\tau} = \boldsymbol{\tau}(\boldsymbol{\vartheta}) \tag{3.6}$$

---

[7] This is because the resolution of the floating point number becomes lower as the exponent gets larger.

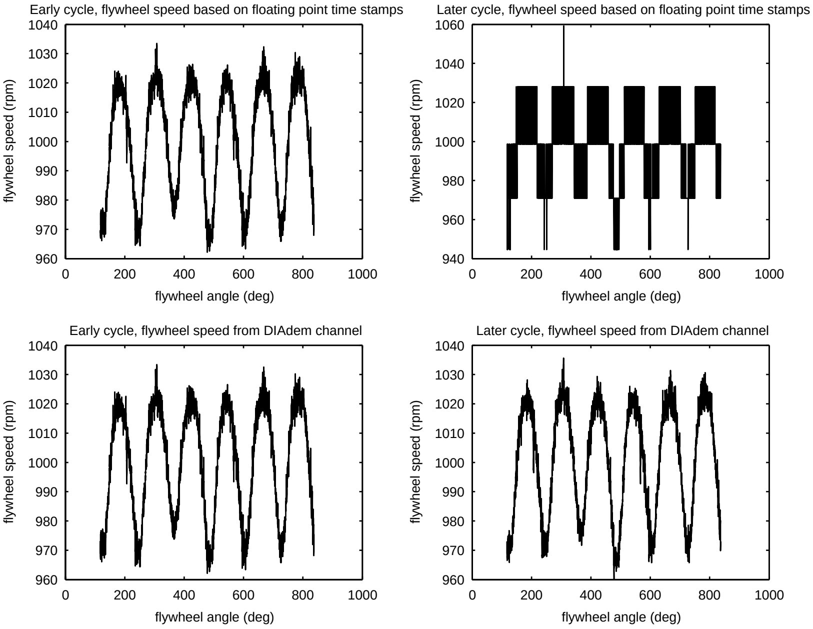

Figure 3.6: *Cancellation phenomenon due to floating-point-number approximation. The two figures on top are flywheel speed based on floating point time stamps. The two bottom figures are from a speed channel in the DIAdem data set—it is not known how it was created. The two left figures show two cycles at the start of the measurement. The two right figures show cycles later in the measurement.*

where $\boldsymbol{\vartheta} = (\vartheta_0 \, \ldots \, \vartheta_M)^T$ and $\vartheta_k = (1-\alpha)\theta_j + \alpha\theta_{j+1}$—see figure 3.7. To transform the pressure signal onto the angular domain we write

$$\boldsymbol{p} = \boldsymbol{p}(\boldsymbol{\tau}) = \boldsymbol{p}\big(\boldsymbol{\tau}(\boldsymbol{\vartheta})\big). \tag{3.7}$$

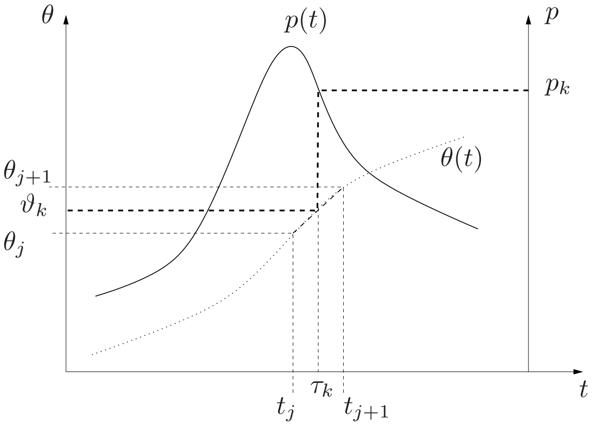

Figure 3.7: *Mapping pressure samples from the time domain onto the angular domain. Linear interpolation is used between θ_j and θ_{j+1} to define ϑ_k.*

The speed signal is constructed using central approximations of the derivative,

$$\begin{aligned} g_i(t) &= \frac{1}{\Delta t_i}\big(\theta(t+\Delta t_i/2) - \theta(t-\Delta t_i/2)\big) \\ \Rightarrow G_i(s) &= \frac{1}{s\Delta t_i/2}\frac{e^{s\Delta t_i/2} - e^{-s\Delta t_i/2}}{2}\mathcal{L}\dot{\theta}(s) \\ \Rightarrow G_i(j\omega) &= \frac{\sin(\omega\Delta t_i/2)}{\omega\Delta t_i/2}\mathcal{L}\dot{\theta}(j\omega), \end{aligned} \tag{3.8}$$

i.e. no frequency is phase shifted compared to the exact derivative, and the magnitude is not significantly changed for lower frequencies. When transforming the constructed speed signal

$$\dot{\boldsymbol{\theta}}(\boldsymbol{t}) = \big(g_0(t_0+\Delta t_0/2), \ldots, g_{n-1}(t_{n-1}+\Delta t_{n-1}/2)\big)^T \tag{3.9}$$

onto the angular domain,[8] it is assumed that

$$\theta(t_i + \Delta t_i/2) \approx \theta(t_i) + \Delta\theta/2 \tag{3.10}$$

is a good approximation.

---

[8] The array is one sample shorter than the time array $\boldsymbol{t}$ since we do not have the value of Δt_n.

3.3.3 A Short Analysis of the Constructed Signals

The results in figure 3.8 show that cycle-to-cycle pressure variations are small. However, different cylinders or engines have not been examined.

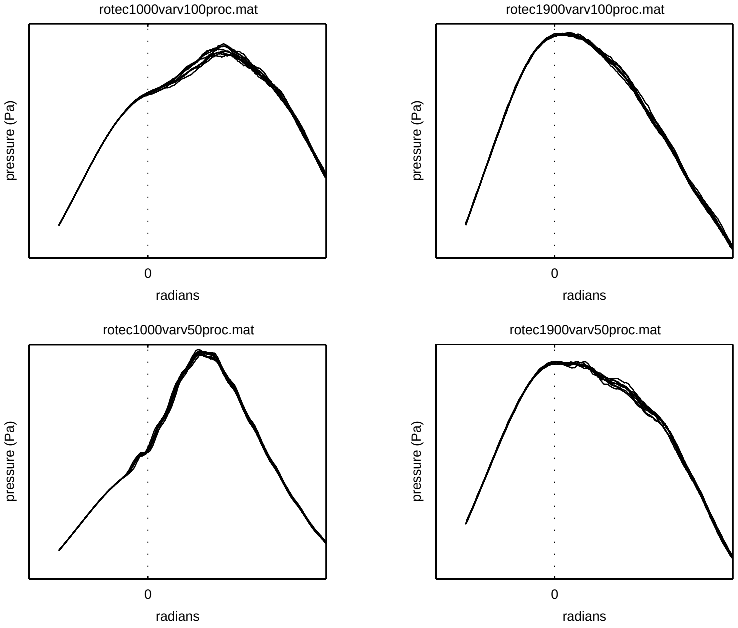

Figure 3.8: Cycle-to-cycle variations of cylinder pressure near TDC at various operating points. The data shown is from the second series of measurements in a test bed, and 10 consecutive cycles are displayed in each plot, even if they are hard to discern. The pressure curves from the first series of measurements give similar plots.

The speed signal that is extracted from Rotec is not smooth which can be seen in figure 3.9. This also occur after compensating for non-equidistant spacing in the circular disc. The noisy signal may be due to imperfections in measurement equipment used.

3.3.4 Reason for the Noisy Speed Signal

There are only 720 markers in the disc, but the TTL signal gives 1800 pulses per revolution—see figure 3.4. The equipment in the measure chain that scales the frequency must extrapolate time stamps in order to enhance resolution in real time. We can use formula (3.2) to roughly estimate that the equipment needs a sample rate of *at least* 10 MHz

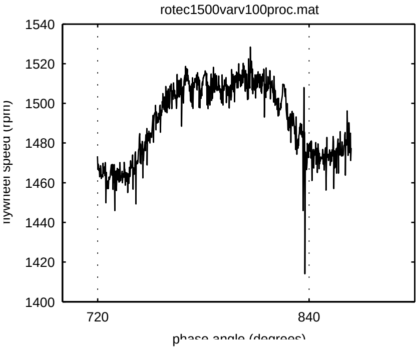

Figure 3.9: *Non-smooth speed signal from Rotec. The figure shows the spike in flywheel speed that the first cylinder gives rise to at 1500 rpm and 100% load.*

to avoid losing information. It should be investigated if the equipment has any positive effects.

3.3.5 A Comparison Between the Speed Signal from S6 and the Speed Signal from Rotec

The main reason for comparing the signal from S6 with the signal from Rotec is to examine if any dynamical differences can be noted.[9] If no major differences are seen, data from Rotec may be used as verification data for the model. The noisy speed signal is not a major problem since the purpose of the model is to correctly model lower order frequencies.[10]

Results from speed comparisons show that the signals are not much different in their dynamical properties at 1500 rpm. The signal from Rotec has a slightly larger magnitude for the third-order frequency, as seen in figure 3.10. Measurements from S6 was only extracted at 1500 rpm.[11] Greater differences at higher speeds are expected. However, this may not be necessary to examine in the future since the signals are cycle-periodic and it is possible to use speed data from S6 and pressure data from Indiscope in the model.

---

[9] Remember from figure 3.1 that Rotec gets its signal from the circular disc attached to the flywheel, whereas S6 measures directly on the flywheel.

[10] It is common practice in automotive engineering to speak about frequency orders. The engine-speed frequency is defined as the first order frequency, the second order frequency is twice as high as the engine frequency, and so on.

[11] This was due to problems with the software used for extracting signals from S6.

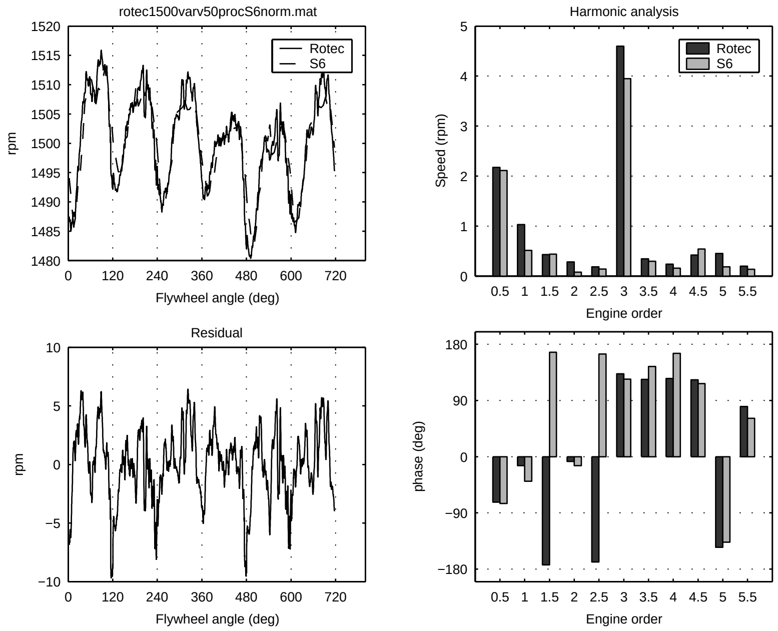

Figure 3.10: *A comparison between signals from S6 and Rotec in the test bed environment at 1500 rpm and 100% load. A difference in the third-order magnitude is seen.*

3.4 Measurements on the Chassis Dynamometer

To examine if different truck drivelines can give rise to different speed responses on the flywheel, speed measurements were carried out on the chassis dynamometer on two different trucks, MIKE and MOA. Figure 3.11 depicts the measurement setup. The trucks have the same engine type, D12, but different drivelines.[12] Test-bed pressure curves for an engine with a similar configuration as the trucks' were found. Hope was that the same injection time, α, and injection angle, δ, would recreate the pressure curves with good accuracy. This would allow to simulate the trucks' flywheel speeds later, if driveline models were available. Table 3.3 shows the map used in the measurements for both trucks.

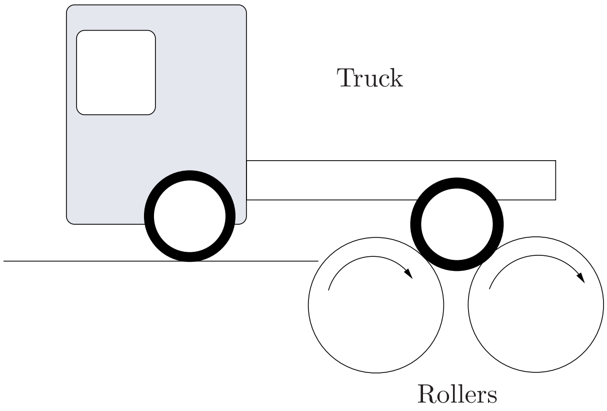

Figure 3.11: *A schematic view of how the chassis dynamometer works. The rollers are connected to dynamometers to provide load torque on the driveline.*

Load	1000 rpm	1500 rpm	1900 rpm
100%	B	B	B
75%	B	B,+1,-1	B
50%	B	B	B
25%	B	B	B

Table 3.3: *Operating points used in the third series of measurements, using the same notation as in table 3.1.*

---

[12] One difference is the length of the propeller shafts.

3.4.1 A Comparison Between the Speeds for the Two Trucks

Speed comparisons show that there is no significant difference in flywheel speed between the two trucks at most operating points, represented by figure 3.12. The only operating point where the trucks show a difference in flywheel speed dynamics is at 1000 rpm and 100% load where Moa has a half-order contribution—see figure 3.13. One reason for this difference could be that a near resonance frequency for Moa's driveline is excited, which then gives a significant torque response back to the flywheel.

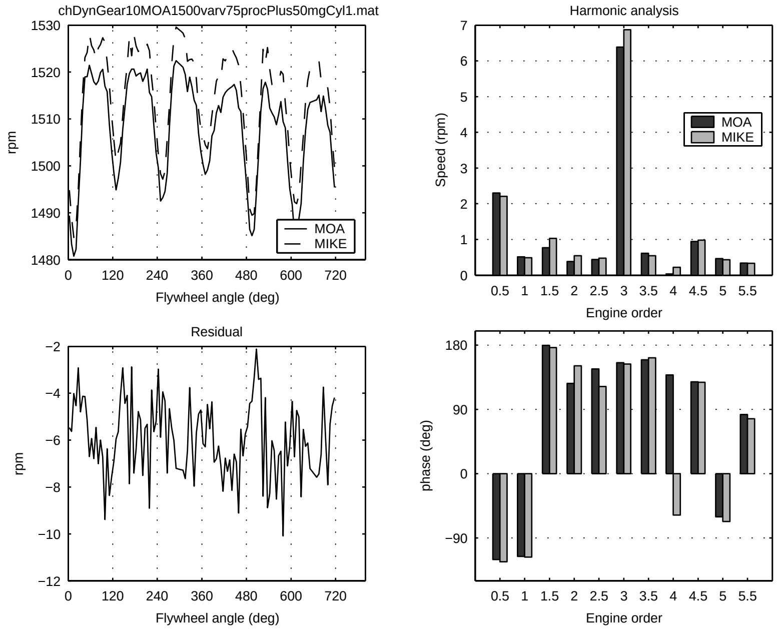

__Figure 3.12:__ A comparison between speeds from the two trucks Mike *(gear 10) and* Moa *at 1500 rpm and 75% load with a positive offset of 50 mg injected fuel in cylinder 1. This example represents how the speeds differ at most operating points.*

3.4.2 A Comparison Between Speeds for the Trucks and Speeds in the Test Bed

Slight differences are seen for most measurements when speed signals from measurements in the test bed and speed signals from measurements at the chassis dynamometer are compared. The difference at

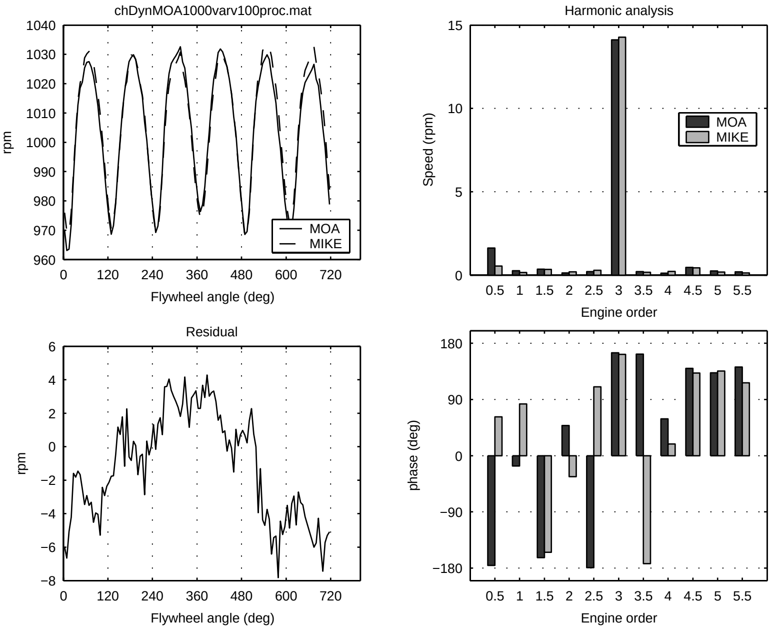

Figure 3.13: *A comparison between speeds from* Mike *and* Moa *at 1000 rpm and 100% load. A significant difference of the half order magnitude can be seen.*

half the engine order at 1500 rpm shown in figure 3.14 probably derives from an excited resonance frequency for the driveline used in the test bed—see chapter 4. However, the higher order differences seen in figure 3.15 at 1900 rpm are probably not only due to driveline differences. It is possible that they result from dynamics between the flywheel and the circular disc in the test bed.

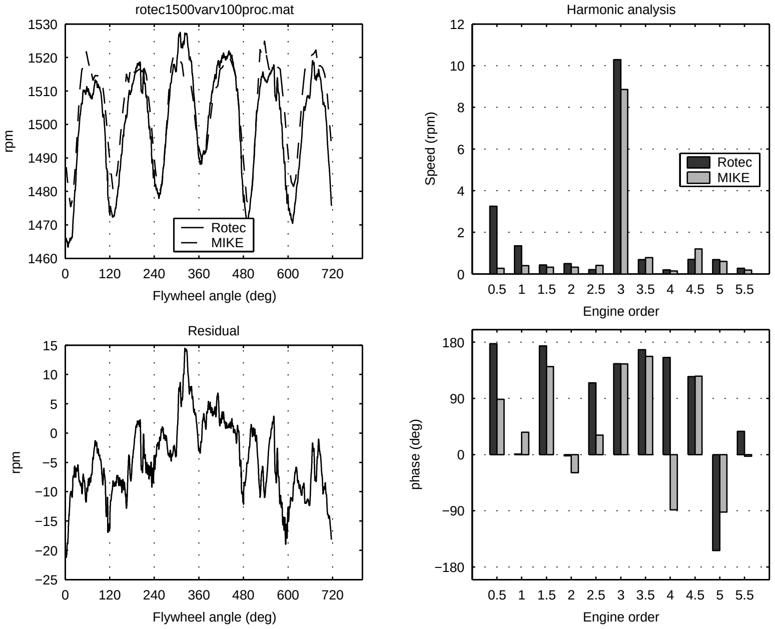

Figure 3.14: *A comparison between speeds from* Mike *and Rotec at 1500 rpm and 100% load. The half-order magnitude in the test-bed signal probably derives from a resonance in the test-bed driveline.*

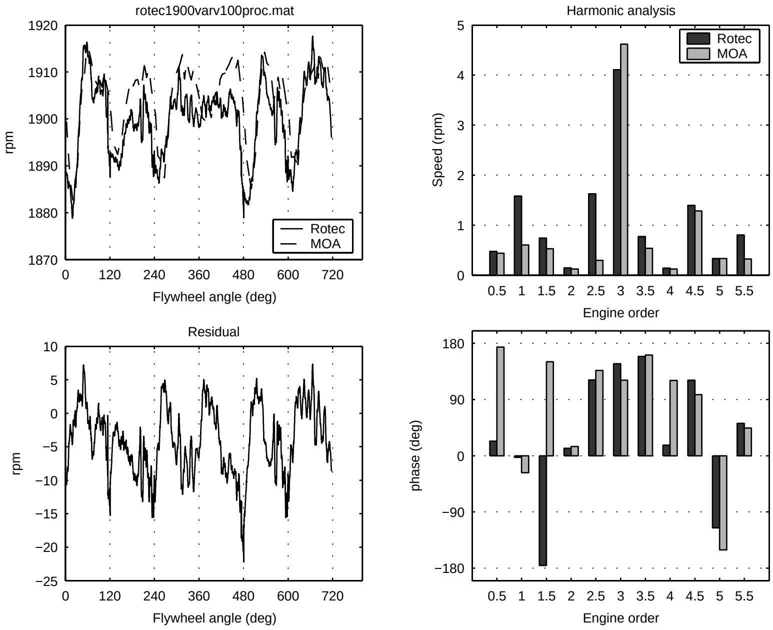

Figure 3.15: A comparison between speeds from Moa *and Rotec at 1900 rpm and 100% load. The speeds differ somewhat at higher orders which indicate dynamics between the flywheel and the circular disc in the test bed.*

Chapter 4

Simulations

Some variations of the model described in chapter 2 were implemented in MATLAB/Simulink using *S*-functions written in *C*. A MATLAB class and a number of *M*-files were constructed to facilitate when running different setups, and when analyzing the simulations—see [12] for more details. The following model variations are discussed in this chapter:

The simple model The model described in chapter 2.

The dynamically equivalent model This model uses a dynamically equivalent model of the connecting rod.

The test-bed driveline model The simple model extended with a simple test-bed driveline.

The truck-driveline model The simple model extended with a simple truck driveline.

Trial-and-error models The simple model with adjusted parameters.

Parameters for the models were fetched from [7, 8, 10] and [1]. There are some uncertainties in the engines' configurations,[1] and the values of many parameters differ slightly between the reports (a relative difference of about 0.15).

Parameter values were fed into the models and simulations were made for all operating points. To estimate the initial state, $\boldsymbol{x}_0$, a preliminary simulation was run to the beginning of a cycle where it was assumed that the transient response had died out. The friction torque (modeled as absolute-damping elements) is unknown and estimated from an energy-balance equation at steady-state conditions.

---

[1] For instance, it is unknown whether *Holset*- or *Hasse & Wrede* dampers were used.

The absolute-damping elements in the model are set thereafter. The absolute-damping elements ranges between 0.06 and 0.8 [Nms/rad] for the 65 possible measurement setups used in this work.

4.1 The Simple Model

The model with nine inertias described in chapter 2 will be referred to as the *simple model*. A simulation at 1000 rpm and 100% load is compared with actual measured data in figure 4.1.[2] It can be seen that the simple model follows the measured data well. Interesting to note are the depths of the dips between the firing of cylinders. The firing sequence of the engine is 1–5–3–6–2–4, where cylinder 1 is the furthest from the flywheel—see figure 2.2. The trend is that the dips are deeper where cylinders that are far from the flywheel fire.

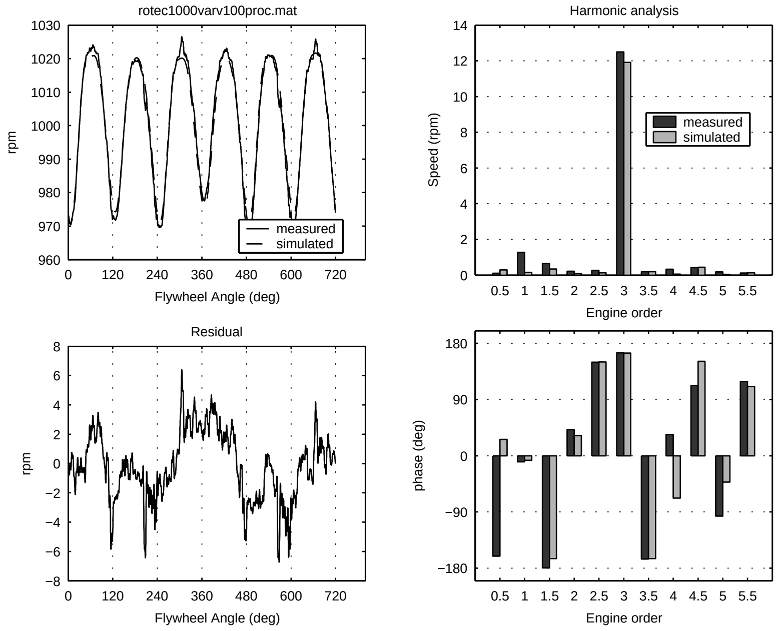

Figure 4.1: *Simulation with the simple model at 1000 rpm and 100% load. The model works well at this operating point.*

The simple model has trouble to follow some dynamics when simulating at 1500 rpm and 100% load as seen in figure 4.2. The largest differences occur for lower-order frequencies where the measured speed has a significant contribution. Section 4.3 indicates that the model needs a driveline to explain the lower-order contributions at this operating point.

---

[2] The time-discrete flywheel speed signal that Simulink returns is not equidistant in angle. Thus, before transforming the signal onto the frequency domain equidistant interpolation is done in the angular domain.

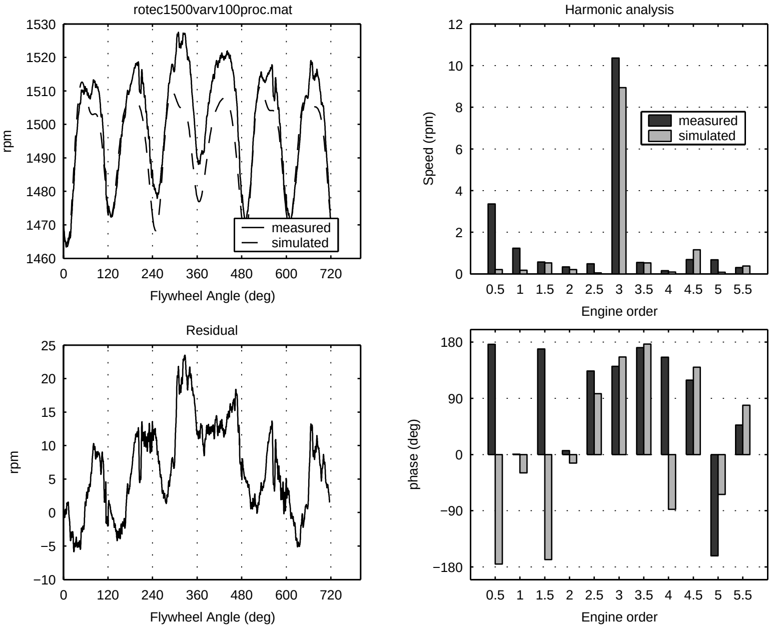

__Figure 4.2:__ Simulation with the simple model at 1500 rpm and 100% load. The measured speed has lower-order contributions that the model can not explain.

Finally, a simulation is made at higher engine speed. It can be seen in figure 4.3 that the model has trouble to follow the measured data here too. However, note that the simulated speed correspond somewhat better to the flywheel speed from MIKE seen in figure 3.15. Again, one reason for the differences can be that there are dynamics to be considered in the test bed between the circular disc and flywheel at higher speeds.

The results from the simulations show that the simple model does not cover all important phenomena that give rise to different vibrations on the flywheel in the test bed.

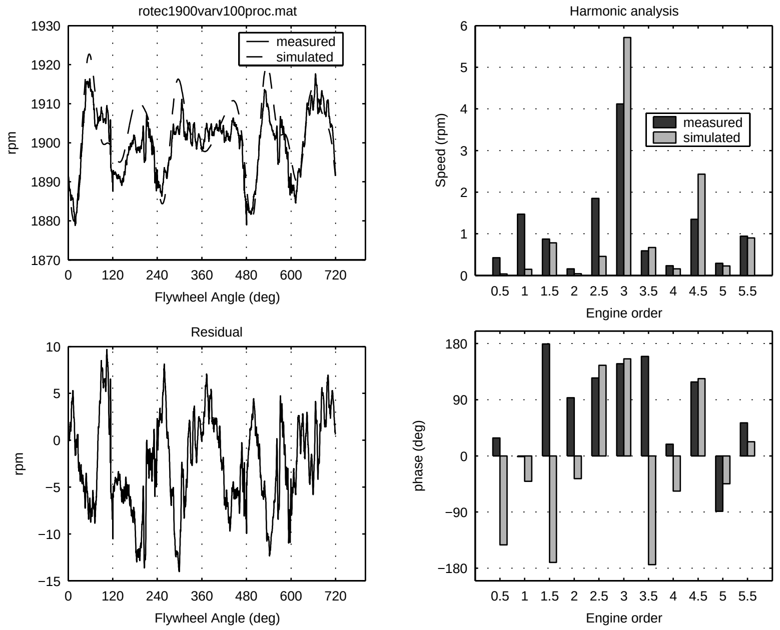

Figure 4.3: *Simulation with the simple model at 1900 rpm and 100% load. The simulation differ from measured data. Remember that the measured data is from the circular disc in the test bed.*

4.2 A Dynamically Equivalent Model of the Crank-Slider Mechanism

The simple model uses a statically equivalent model of the crank-slider mechanism. Schagerberg and McKelvey [14] refer to papers by Hafner and Shiao respectively where error analysis between statically- and dynamically equivalent models are performed. Still, a dynamically equivalent model was implemented and compared to the simple model. The equations for a dynamically equivalent model are derived in appendix A.1.

An approximate value of the connecting rod was used. A comparison between models at 1900 rpm is seen in figure 4.4. No major differences are seen between simulations with the simple model and the dynamically equivalent model, and it is from here on assumed that there is no need for a dynamically equivalent model of the crank-slider mechanism, even though an approximate value for the moment of inertia of the connecting rod was used.

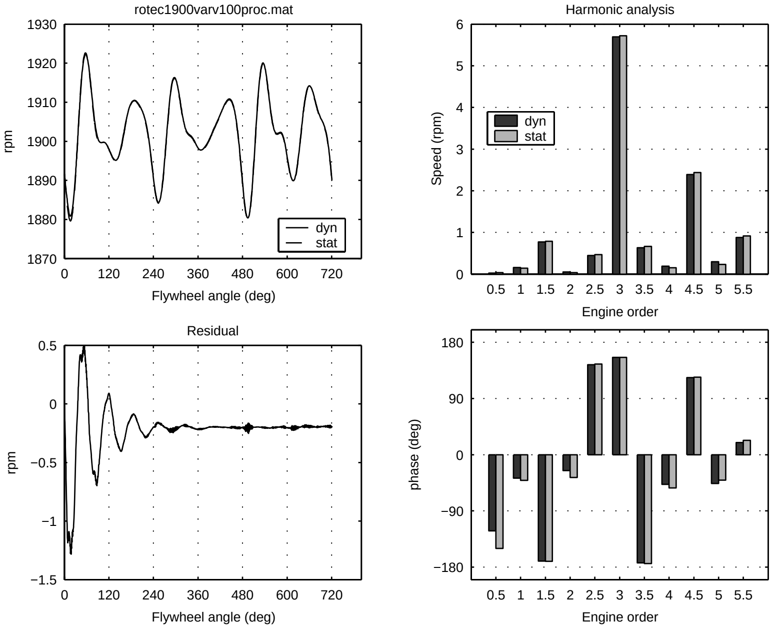

Figure 4.4: *A comparison between statically- and dynamically equivalent models at 1900 rpm shows that a statically equivalent model of the connecting rod is sufficient for simulation.*

4.3 Including a Model of the Driveline

The simple model was not accurate at operating points other than at low engine speeds (1000 rpm and 1250 rpm), and there were no improvements when using a dynamically equivalent model for the crank-slider mechanism. The half-order frequency at 1500 rpm may be due to responses from the driveline in the test bed environment, so the next step will be to include a simple driveline in the model.

The major thing that changes in the model when a driveline is included is the number of elements included in the lumped-mass model, see figure 4.5. Conversion ratios for the transmission and final drive are included by manipulating the damping- and stiffness matrix, $\boldsymbol{C}$ and $\boldsymbol{K}$, as described in section A.2.

Parameters for a simple test-bed driveline can be found in [7]. It takes many cycles for the transient to die out when we include this driveline model as can be seen in figure 4.6. In all simulations in this section, 30 cycles were simulated before an initial state was estimated.

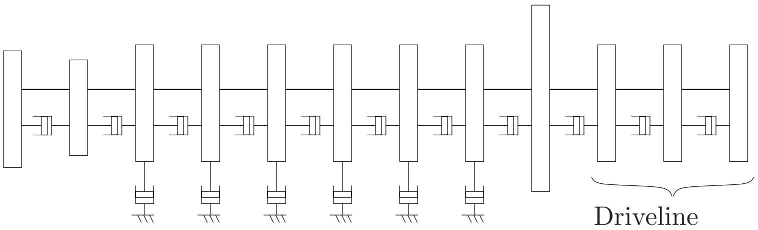

Figure 4.5: *The lumped mass model including a simple driveline.*

Simulations with the driveline model show no major differences from the simple model at 1000 rpm and 1900 rpm. This is probably because the driveline is not forced near a resonance frequency at these operating points. On the other hand, at 1500 rpm the driveline model differs significantly from the simple model. In figure 4.7, a simulation at 1500 rpm is compared with actual measured data. This is an operating point where the simple model had trouble following the lower-order frequencies. It can be seen that the extended model follows the measured data better which indicates that the test-bed driveline responds significantly near 1500 rpm. The parameters used also show that the driveline has a resonance frequency with low damping near 750 rpm, which is the half order frequency of 1500 rpm.

Another operating point at 1500 rpm is simulated to further investigate the driveline model. The simulation is compared with actual measured data where cylinder 5 has a positive injection offset. This means that we are forcing the driveline at its resonance frequency. It

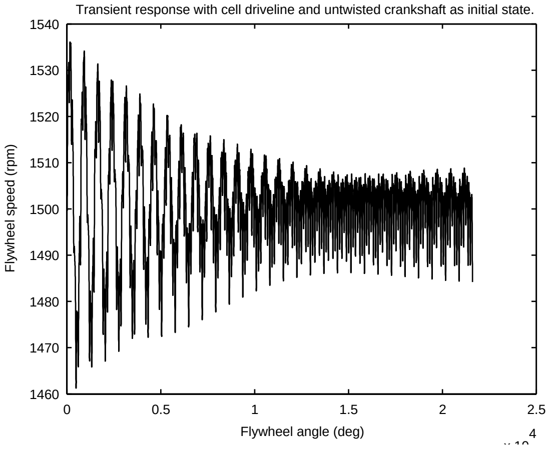

__Figure 4.6:__ It takes a number of cycles for the transient response to die out when including a test-bed driveline. This figure shows the first 30 cycles from a simulation.

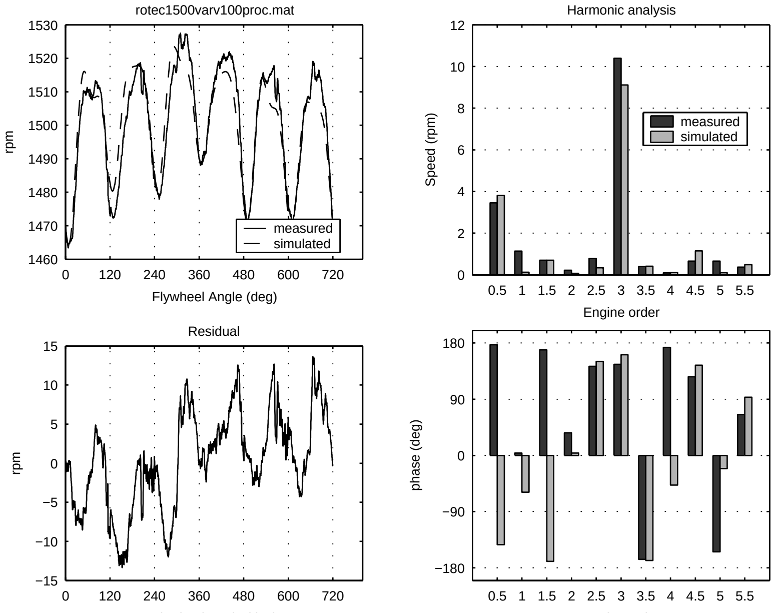

__Figure 4.7:__ Simulation with the driveline model at 1500 rpm and 100 % load. This model can explain the lower-order contribution.

can be seen in figure 4.8 that the simulated data is nowhere near the measured data. This may be due to limitations in the driveline model. It is for instance unlikely that the test-bed engine actually has a transient response such as in figure 4.6.

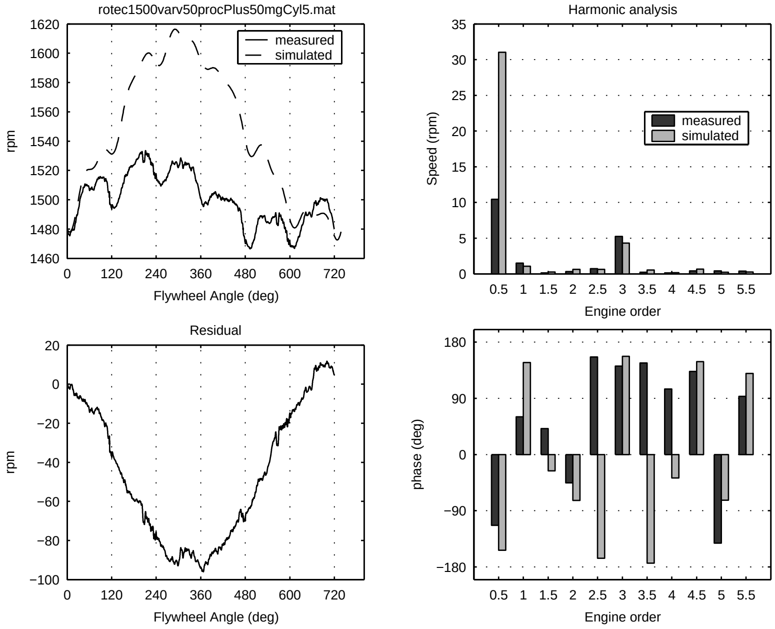

Figure 4.8: *Simulation with the driveline model at 1500 rpm and 100 % load with a positive pressure offset present in cylinder 5.*

4.4 A Truck-Driveline Model

Section 3.4 shows no indications of significant torque responses from truck drivelines. To further investigate this matter, a simple truck driveline was implemented and simulated at various operating points. Parameters for the driveline are estimated for the truck MALTE by Berndtsson and Uhlin [4]. The value of the flywheel inertia was adjusted to get better simulation results.

The lowest resonance frequency in the driveline model is higher than 1900 rpm, and more damped than the resonance frequency for the test-bed driveline model. It is hard to estimate if the driveline will contribute to dynamics at higher orders, but there should not be any major contributions at lower orders.

4.4.1 Simulations with a Truck Driveline Compared to Simulations Without a Driveline

Simulations with and without a driveline in the model were performed, and comparisons are shown in figures 4.9 and 4.10. Differences are most significant in simulations at the third-order frequency. This can be due to a wrongly estimated flywheel inertia. The value of a *significant* lower-order difference is not known. However, section 4.4.2 shows that the results should be questioned.

One thing that still should be investigated is the half-order contribution for MOA at 1000 rpm and 100% load—see section 3.4.1. It is the only measured operating point that indicates a significant torque contribution from a truck's driveline.

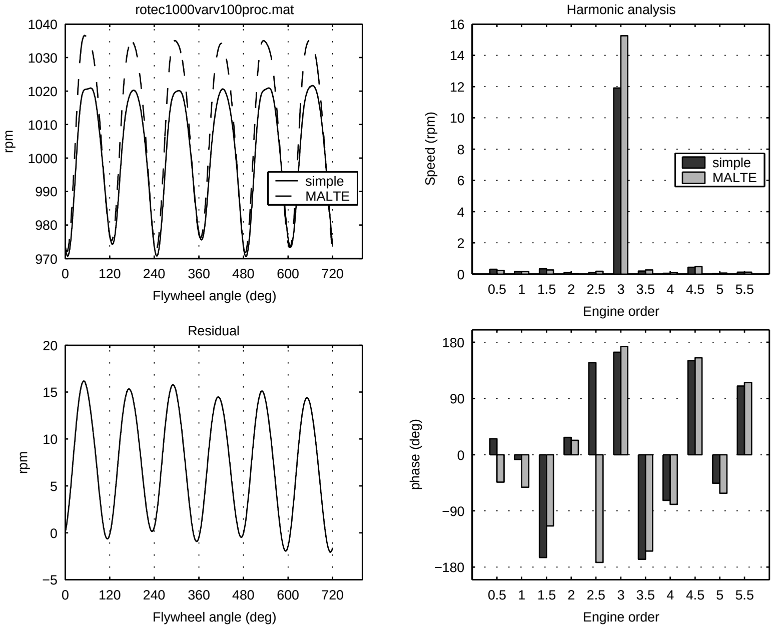

Figure 4.9: *A simulation at 1000 rpm with a truck-driveline model for* Malte *compared to one with no driveline.*

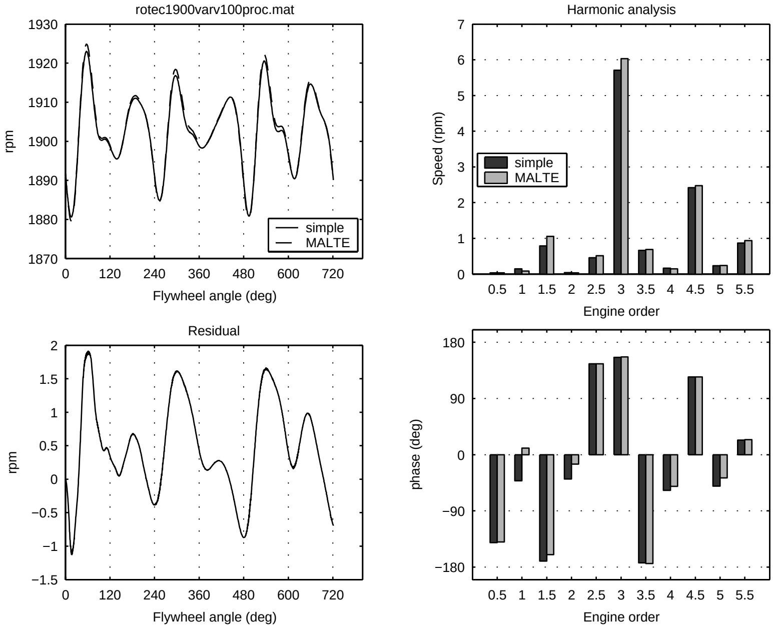

Figure 4.10: *A simulation at 1900 rpm with a truck-driveline model for* Malte *compared to one with no driveline.*

4.4.2 Simulations with a Truck Driveline Compared to Measured Data

Figures 4.11 and 4.12 show comparisons between simulations and measurements carried out at the chassis dynamometer.

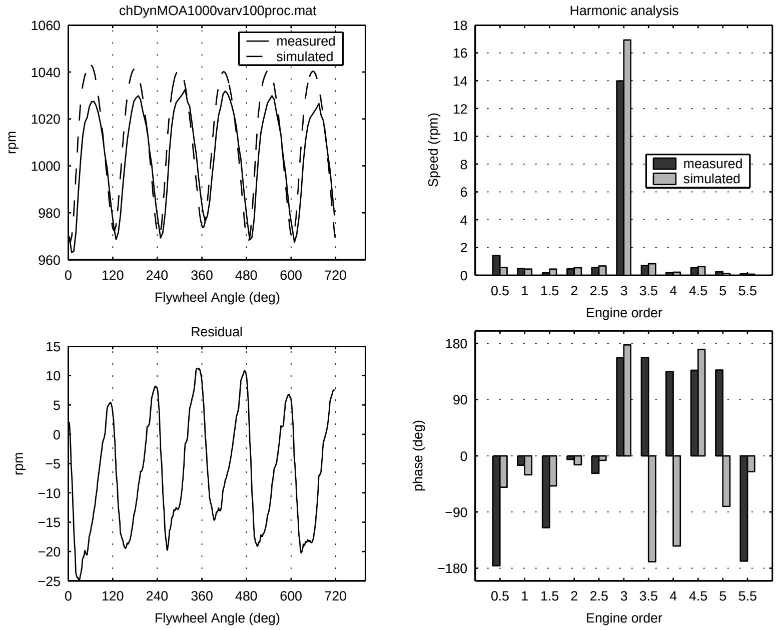

Figure 4.11: *A simulation at 1000 rpm with a truck-driveline model for* Malte *compared to measured flywheel speed from* Moa.

The speeds from the trucks are significantly phase shifted compared to the simulations. This phenomenon also occur when the simple model is used for simulating the trucks. One suggested reason is uncertainties in TDC position when the pressure curves for the measurements was made, but this is not confirmed when the pressure curves are plotted.[3] Another reason could be that the time stamps do not begin exactly at TDC for cylinder 1, but this should still not result in such a large phase shift. The discussion in section 4.4.1 should be read critically since the model can not follow measured speed.

---

[3] Remember that the pressure curves for the truck simulations are from stored data, see section 3.4.

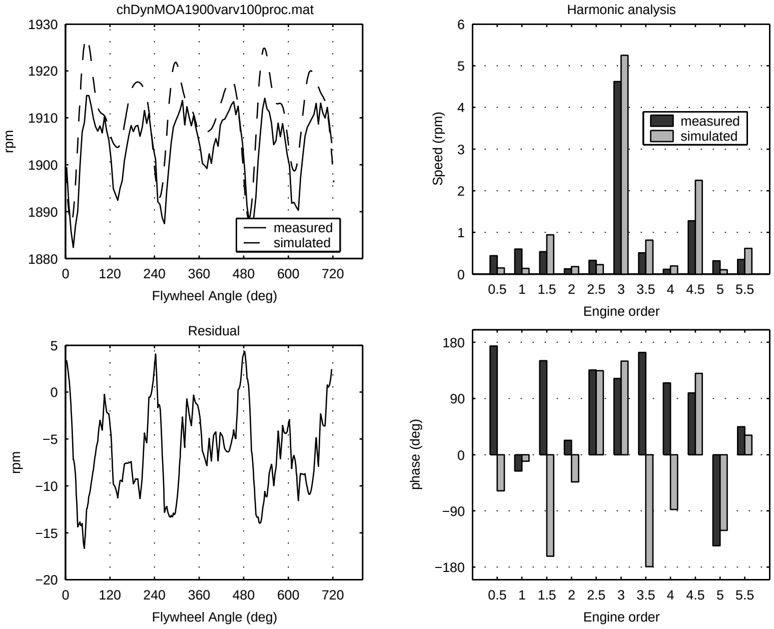

Figure 4.12: *A simulation at 1900 rpm with a truck-driveline model for* MALTE *compared to measured flywheel speed from* MOA.

4.5 Trial-and-Error Modeling

All recent models have trouble at higher engine speeds. In this section parameters are altered manually to see if a better model can be found.

4.5.1 An Alternative Damper Model

As seen from figures in previous sections, each power stroke from the firing of the cylinders creates a torque spike on the crankshaft. These torque spikes cause the crank journal to twist slight and spring back, causing torsional vibrations in the crankshaft. A vibration damper is mounted to the front of the crankshaft to reduce the damaging effect of these vibrations.

Dampers in Scania's trucks use viscous fluid to dampen torsional vibrations. In general, the motion of fluids is complicated which makes it reasonable to believe that the model of the damper can be improved.

In the simple model, the damper is modeled as two lumped masses connected with a linear spring and damper. A more general model of the damper torque is not restricted to linear dependencies only. In one trial-and-error model of the damper, the function

$$T_d(\theta_{1-2}, \dot{\theta}_{1-2}) = k_1\theta_{1-2} + c_1\dot{\theta}_{1-2} + k_2\sqrt{\theta_{1-2}} + c_2\dot{\theta}_{1-2}^2 \tag{4.1}$$

was used for the damper torque T_d, where the parameters were set by trial and error.[4] The arguments θ_{1-2} and $\dot{\theta}_{1-2}$ are the angular- and speed difference respectively between the two lumped masses in the damper model. Simulations were carried out at various parameter choices and one result is shown in figure 4.13.

It is not known what constitutes a reasonable model of the damper, but different setups in damper parameters result in slightly different results in simulations compared to the simple model. Yet, it has not been shown that the problem at higher speeds derives from limitations in the damper model, and the trial-and-error model is not significantly better at any tried parameter setup.

4.5.2 Manipulating Parameters Based on Simulation Experience

In the simulation shown in figure 4.14 the crankshaft stiffness was multiplied by 1.3 compared to the crankshaft stiffness in previous models. Simulations follow dynamics at 1900 rpm better in this case.[5] Still, the simulated data is phase shifted compared to measured data. This can

---

[4] The aim of the function was to let torque due to difference in position be *less* significant at larger angle differences, whereas torque due to speed difference should be *more* significant at larger speed differences.

[5] In fact, the only significant difference between the signals is a phase shift.

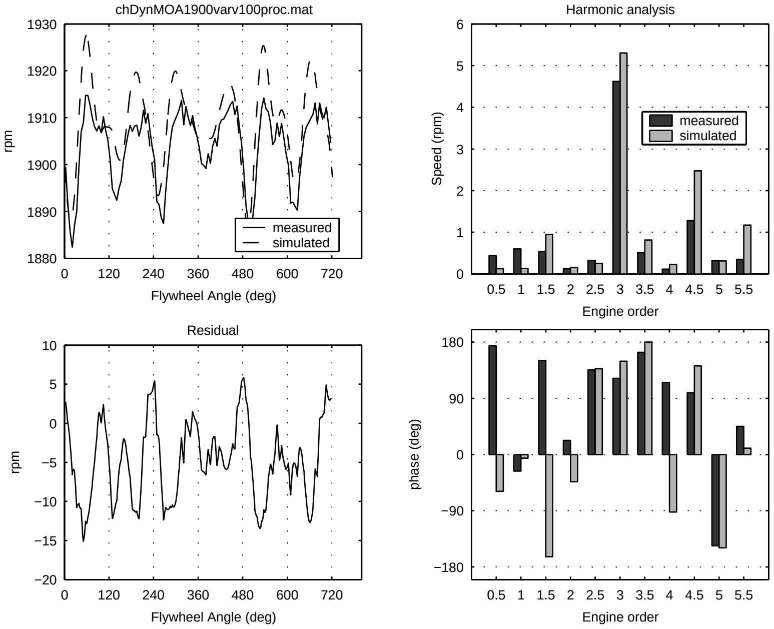

Figure 4.13: *The results turn out somewhat different when another model for the damper is used. The linear parameters k_1 and c_1 are set to zero in this particular simulation, while $k_2 = 5000$ [Nmrad$^{-1/2}$] and $c_2 = 100$ [Nms^{2}rad^{-2}].*

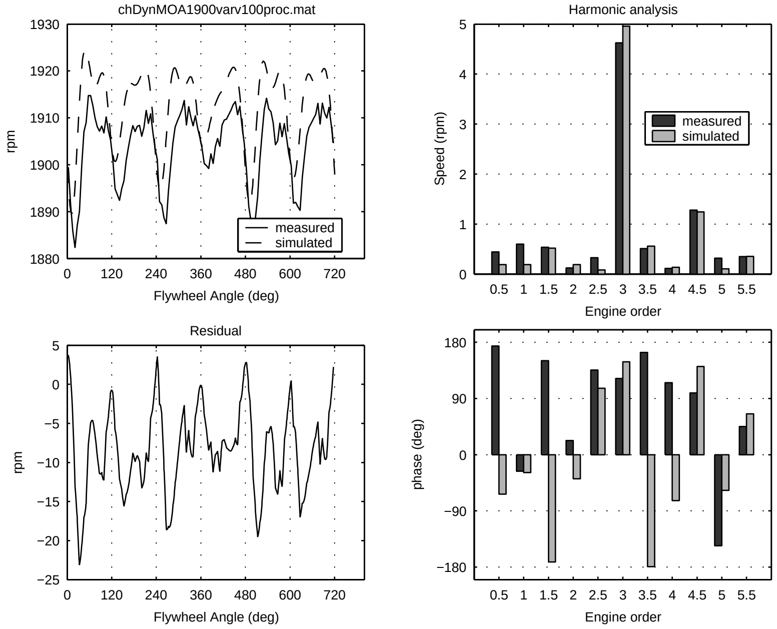

Figure 4.14: *A simulation with modified stiffness parameters. The only significant difference is a phase shift.*

be corrected to a certain degree by for instance weakening the stiffness between the last cylinder and the flywheel, but this will at the same time slow down dynamics. By comparison, this model is in some sense the closest to measured data. However, it is not known if the parameter values are reasonable.

Optimization of parameters based on measured data from S6 may lead to an acceptable model in the future. The drawback with this method is that it may require repeating the optimization procedure for new engine configurations.

4.6 Sensitivity Analysis

Simulated data has not corresponded to measured data at higher speeds. Could uncertainties in model parameters contribute to the errors? To examine this, simulations at 1900 rpm for models with perturbed parameters were made.

First, cylinder pressures that are used as input in the model are perturbed. This is done in three ways. The pressure curve is first scaled, then it is offset and last it is translated in θ to see if it makes a big difference in the model output.[6] These perturbations mimic possible errors when measuring pressure.

After perturbing the pressure curves we alter other parameters in the model. First we alter the inertias and then we alter the stiffness parameters. The parameters have been altered by a relative fraction of 0.2. Results are seen in figures 4.15–4.19.

We altered parameters for the damper in section 4.5.1. It is unknown if those changes are reasonable.

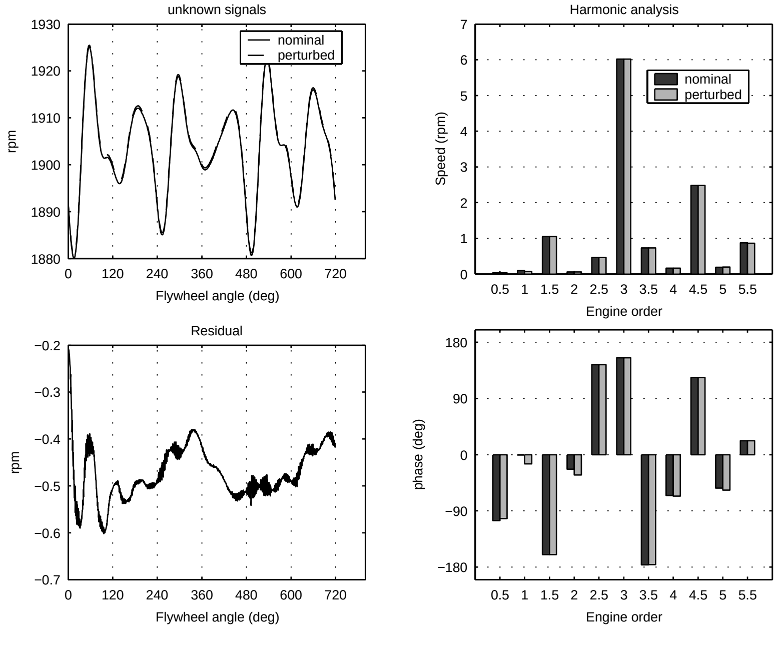

Figure 4.15: *A comparison between simulations where one simulation has its pressure curve offset by -5 bars.*

---

[6] The absolute damping are set different in the two models, to compensate for different work contributions from the pressure curves.

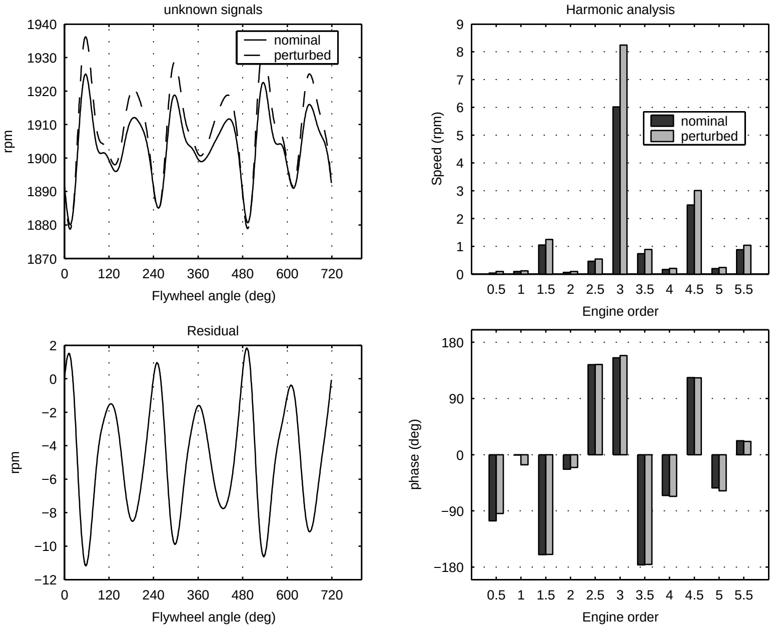

Figure 4.16: *A comparison between simulations where one simulation has its pressure curve scaled by a relative fraction of 0.1.*

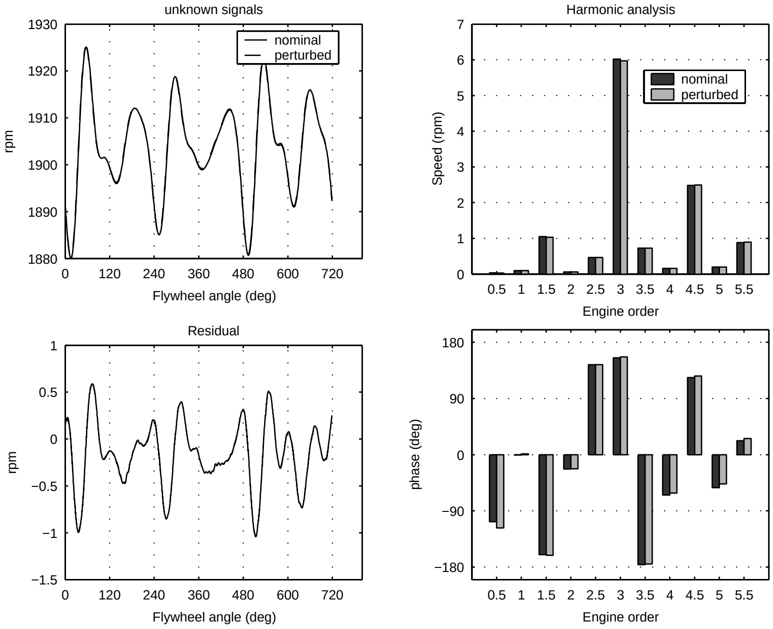

Figure 4.17: *A comparison between simulations where one simulation has its pressure curve translated 1° to the left.*

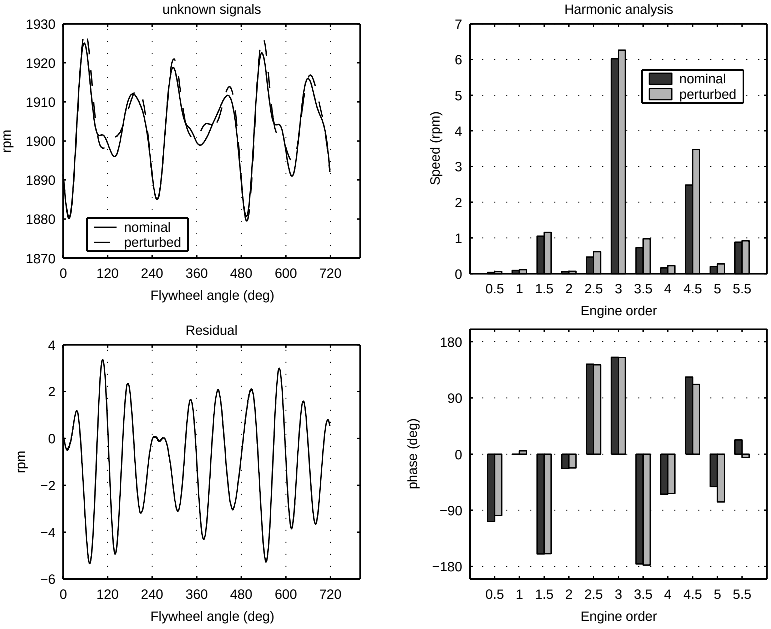

Figure 4.18: *A comparison between simulations where one simulation has its stiffness parameters of the crankshaft and driveline perturbed by a relative fraction of 0.2.*

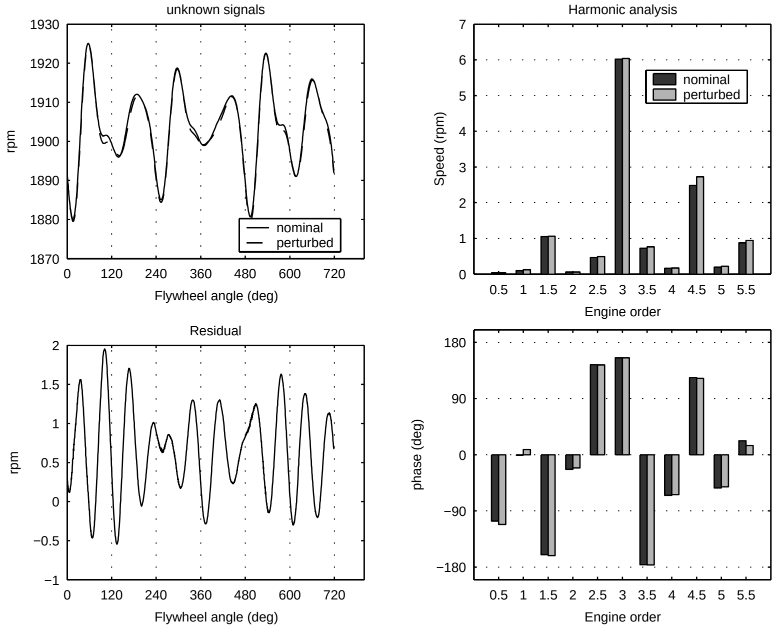

Figure 4.19: *A comparison between simulations where one simulation has its inertias of the crankshaft and the driveline perturbed by a relative fraction of 0.2.*

The sensitivity analysis indicates that the model is most sensitive to scaled pressure and offset stiffness parameters. More experience is needed to judge if the model is robust enough to find adequate parameter values, but nothing yet indicates the opposite.

Chapter 5

Conclusions

5.1 Conclusions from the Measurements

Pressure curves from the measurements do not differ much from cycle to cycle and there does not appear to be significant contributions of frequencies lower than half order at steady-state conditions. This, together with the sensitivity analysis in section 4.6 indicate that it is possible to find a model that can facilitate to gain understanding of the transfer function discussed in chapter 1.

Measurements in the test-bed environment indicate that the test-bed driveline has a resonance frequency near 750 rpm that affects flywheel speed variations when excited. The two speed signals from S6 and Rotec are not significantly different at 1500 rpm, but could differ more at higher speeds.[1] Measurements from the chassis dynamometer support this, if we assume that speeds from trucks are similar to speeds in the test-bed environment. This may not be necessary to investigate since the speeds are cycle-periodic and it is possible to use speed from S6 and pressure curves from Indiscope.

Measurements on MIKE and MOA show that both flywheels have similar speed variations at similar operating points, indicating that a driveline could be omitted in the model when simulating trucks. Nevertheless, at 1000 rpm and 100% load there is a slight difference.

Flywheel speed fluctuations in the test bed look similar to fluctuations in the chassis dynamometer. Still, they differ more at higher speeds. This may be due to different engine configurations, but it is more likely due to dynamics between the flywheel and the circular disc in the test-bed environment.

More accurate signals may be obtained with Rotec if the frequency scaler is omitted in the measure chain. It should be examined if the frequency scaler used in test beds have any positive effects. Still, the signals obtained are accurate enough to test and verify the model.

---

[1] Remember that we were only able to extract the S6 signal at 1500 rpm in the test-bed environment.

5.2 Conclusions from the Simulations

The simple model follows the measured speed signal well at low speeds, while it has trouble at higher speeds. Simulations with a dynamically equivalent model for the crank-slider mechanism do not differ from simulations with the simple model, indicating that a statically equivalent model of the crank-slider mechanism is sufficient for simulation.

An extended model with a simple test-bed driveline supports the measured indication of a resonance frequency near 750 rpm. However, the model has limitations as shown in figure 4.8.

Simulations with driveline parameters optimized for MALTE differ somewhat from simulations with the simple model. But since the simple model follows measured data better than the model for MALTE the results should not be treated seriously.

Other models were investigated using parameters set after experience. A different model for the vibration damper was used in simulations, giving slightly different results in flywheel-speed variations. Yet, it was not shown that the problems derive from an inaccurate damper model. A model with a stiffer crankshaft was also investigated, showing promise at higher engine speeds, but its speed signals are still phase shifted compared to measured data.

Auxiliary systems, such as the cam shaft, are not taken into consideration in the model. The model is also limited by the number of lumped masses included. It may turn out that this is a fundamental limitation, but it is hard to investigate.

Chapter 6

Future Work

Gathered measurements can be used together with optimization to find better parameters for the model. If more measurement data is needed, it is suggested that extracted data from S6 are used together with pressure curves from Indiscope.[1] However, operating near 1500 rpm in test beds should be avoided, or measurements should be conducted on trucks. If the model continues to have problems at higher engine speeds it is suggested that an alternative model for the damper is investigated. Measuring speed at the damper case could then be of importance.

Another thing to investigate is how much pressure curves differ for different engine configurations and if this has to be taken into consideration in simulations. Examining effects from *Turbo Compound*[2] is also a future issue.

The present work can not answer with certainty if drivelines affect variations in the speed signal for trucks or not. The driveline model for MALTE indicates differences but then the simple model is better than the model for MALTE when simulations are compared with measurements. Finding better parameters in the driveline models may be an issue for the future.

The code in the S-functions can be updated to improve simulation speed. A model for this purpose can be found in [14] and general issues on speeding up S-functions can be found in e.g. S-function templates in MATLAB.

If an adequate model is found in the future, it can be made modular and incorporated in a larger model that includes auxiliary systems of the engine. It may also be used to investigate methods of discovering unbalanced cylinders.

---

[1] This is only because it is simpler than using Rotec.

[2] Turbo Compound uses exhaust gas flow to provide extra torque on the crankshaft.

References

[1] Parameters for Dampers Used in Scania 12 L Engines. Not Published. Received from Johan Lundqvist.

[2] Description of the Data formats and Data set Properties of DIA*dem*—The PC-Workshop. Downloadable from `www.sesystem.co.kr/diadem/image/dmheader.pdf`, 2003. ©GfS mbH Aachen, Germany.

[3] Protokoll: 17-414-029. Internal protocol at Scania, October 2003.

[4] M. Berndtsson and E. Uhlin. Skattning och aktiv dämpning av drivlinesvängningar i lastbil. Master's thesis, LuTH, 2003.

[5] L. Jianqiu and Y. Minggao. Analysis of the Influence of Crankshaft Vibration Upon the Instantaneous Flywheel Speed. *FISITA World Automotive Congress*, 2000.

[6] L. Jianqiu, Y. Minggao, Z. Ming, and L. Xihao. Individual Cylinder Control of Diesel Engines. *Society of Automotive Engineering*, (2002-01-0199).

[7] E. Jorpes. Beräkningsrapport: Torsionssimulering av DL. *Internal Scania Report*, 2001.

[8] E. Jorpes. Beräkningsrapport: Utredning av torsionsfenomen i ny motorprovcell. *Internal Scania Report*, 2002.

[9] U. Kiencke and L. Nielsen. *Automotive Control Systems*. Springer-Verlag, 2000.

[10] J. Lundqvist. Tröghetsmoment sammanställning 030605. Not published.

[11] L. Nielsen and L. Eriksson. *Course material Vehicular Systems*. Bokakademin, 2002.

[12] M. Nilsson. Manual for MATLAB Related Folders. Not published, 2004.

[13] M. Pettersson. *Driveline Modeling and Control.* PhD thesis, Linköpings Universitet, 1997.

[14] S. Schagerberg and T. McKelvey. Instantaneous Crankshaft Torque Measurements—Modeling and Validation. *Society of Automotive Engineering*, (2003-01-0713):2–6.

[15] M. Schmidt, F. Kimmich, H. Straky, and R. Isermann. Combustion Supervision by Evaluating the Crankshaft Speed and Acceleration. *Society of Automotive Engineering*, (2000-01-0558).

Appendix A

Equations for Extended Models

A.1 A Dynamically Equivalent Model of the Connecting Rod

To get to a model with a dynamically equivalent model of the connecting rod, we derive its mass-torque contribution on the crankshaft axis. The crank-slider mechanism has only one degree of freedom, θ. According to Kiencke and Nielsen [9] we have

$$\frac{d}{dt}E = \frac{dE}{d\theta} \cdot \frac{d\theta}{dt} = T\dot{\theta} \tag{A.1}$$

where E is the kinetic energy of the connecting rod, and T is its mass-torque contribution.[1] We can use figure A.1 to derive the mass-torque contribution from the connecting rod. First of all, we see that

$$\varphi = \arctan\Big(\underbrace{\frac{r\sin\theta}{r + l - (s + r\cos\theta)}}_{f(\theta)}\Big).$$

Denoting the argument to the arctan function by $f(\theta)$ and deriving with respect to time gives

$$\dot{\varphi} = \frac{f'(\theta)\,\dot{\theta}}{1 + f(\theta)^2}$$

and

$$\ddot{\varphi} = \frac{1}{1 + f(\theta)^2}\bigg(\Big(f''(\theta) - 2\,\frac{f(\theta)f'(\theta)}{1 + f(\theta)^2}\Big)\,\dot{\theta}^2 + f'(\theta)\,\ddot{\theta}\bigg).$$

---

[1] This equation has not been verified rigorously.

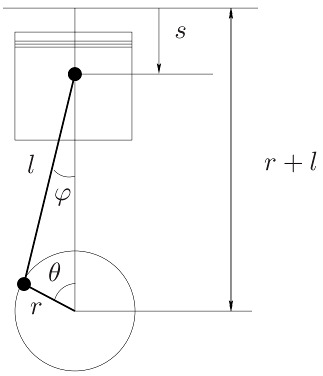

Figure A.1: *The crank-slider mechanism*

Further, we can now express the torque from the connecting rod by deriving

$$E = \frac{1}{2}\,mv^2 + \frac{1}{2}\,J\dot{\varphi}^2$$

with respect to time, which gives

$$\begin{aligned}
\frac{d}{dt}E &= mv\dot{v} + J\dot{\varphi}\ddot{\varphi} \\
&= m\Bigg(\Big\{(1-a)^2r^2 + 2\,(1-a)ar\,\frac{ds}{d\theta}\sin\theta + a^2\Big(\frac{ds}{d\theta}\Big)^2\Big\}\,\ddot{\theta} + \\
&\qquad \Big\{(1-a)ar\,\Big(\frac{d^2s}{d\theta^2}\sin\theta + \frac{ds}{d\theta}\cos\theta\Big) + a^2\frac{ds}{d\theta}\frac{d^2s}{d\theta^2}\Big\}\,\dot{\theta}^2\Bigg)\,\dot{\theta} + \\
&\quad J\frac{f'(\theta)}{(1+f(\theta)^2)^2}\Big(f'(\theta)\,\ddot{\theta} + \Big\{f''(\theta) - 2\frac{f(\theta)f'(\theta)^2}{1+f(\theta)^2}\Big\}\,\dot{\theta}^2\Big)\,\dot{\theta},
\end{aligned}$$

where a is the distance from the big end of the connecting rod to its center of gravity, in fraction of the length of the connecting rod. The mass-torque contribution from the connecting rod can now be identified. For completion, the derivatives of f are

$$f'(\theta) = \frac{r + l - sr\cos\theta + \frac{ds}{d\theta}r\sin\theta}{\big(r + l - (s + r\cos\theta)\big)^2}$$

and

$$\begin{aligned}
f''(\theta) &= r\frac{(\frac{d^2s}{d\theta^2} + s - l + r)\sin\theta}{\big(r(\cos\theta - 1) + s - l\big)^2} \\
&- 2\,r\,\frac{\big((l + r - s)\cos\theta + \sin\theta\frac{ds}{d\theta} - r\big)(\frac{ds}{d\theta} - r\sin\theta)}{\big(r(\cos\theta - 1) + s - l\big)^3}.
\end{aligned}$$

The expressions for the derivatives of the piston displacement s may be found in [9].

By collecting parts multiplying angular acceleration and angular velocity squared respectively, it is quite straightforward to get to a state-space description of the system in the same way as in section 2.5.

A.2 Description of a Simple Truck-Driveline Model

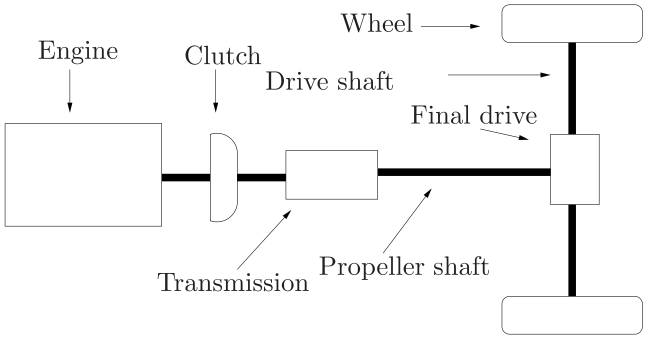
Wheel
Engine
Clutch
Drive shaft
Final drive
Transmission
Propeller shaft

Figure A.2: *A driveline of a rear driven vehicle.*

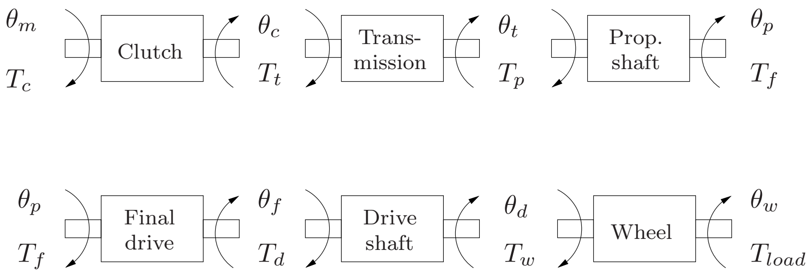
θ_m
T_c
Clutch
θ_c
T_t
Trans-mission
θ_t
T_p
Prop. shaft
θ_p
T_f
θ_p
T_f
Final drive
θ_f
T_d
Drive shaft
θ_d
T_w
Wheel
θ_w
T_{load}

Figure A.3: *Free-body diagrams of parts in the driveline. T stands for torque while θ stands for crank angle.*

A sketch of a driveline is depicted in figure A.2. The equations of motion are found by constructing free-body diagrams of the different parts of the driveline, such as in figure A.3. To illustrate the method, let's work out the equation for the final drive. In the model for MALTE, the final drive has an inertia, J_f, and is characterized by the conversion ratio, i_f, with relations

$$\begin{aligned} i_f T_f &= T_d && \text{(A.2)} \\ \theta_p &= i_f \theta_f. && \text{(A.3)} \end{aligned}$$

The propeller shaft is modeled as an inertia-free spring and damper with stiffness k_p and damping c_p. The same applies to the drive shaft with stiffness k_d and damping c_d. With use of the free-body diagrams and the relations above we get the equation

$$\begin{aligned} J_f \ddot{\theta}_f &= i_f T_f - T_d \\ &= i_f \big(k_p(\theta_t - \theta_p) + c_p(\dot{\theta}_t - \dot{\theta}_p) \big) \\ &\quad + k_d(\theta_d - \theta_f) + c_d(\dot{\theta}_d - \dot{\theta}_f) \\ &= i_f k_p \theta_t - i_f^2 k_p \theta_f + i_f c_p \dot{\theta}_t - i_f^2 c_p \dot{\theta}_f \\ &\quad + k_d \theta_d - k_d \theta_f + c_d \dot{\theta}_d - c_d \dot{\theta}_f. \qquad \text{(A.4)} \end{aligned}$$

Equation (A.4) may be written as

$$\begin{aligned} J_f \ddot{\theta}_f &= \begin{pmatrix} i_f k_p & -(i_f^2 k_p + k_d) & k_d \end{pmatrix} \begin{pmatrix} \theta_t \\ \theta_f \\ \theta_d \end{pmatrix} \\ &+ \begin{pmatrix} i_f c_p & -(i_f^2 c_p + c_d) & c_d \end{pmatrix} \begin{pmatrix} \dot{\theta}_t \\ \dot{\theta}_f \\ \dot{\theta}_d \end{pmatrix}. \qquad \text{(A.5)} \end{aligned}$$

It is straightforward to set up equations for parts in the driveline model and eliminate variables to obtain a system of equations in the same form as in equation (2.6). The difference now is that the block matrices added to $\boldsymbol{K}$ and $\boldsymbol{C}$ by each stiffness- and damping element no longer have to be symmetric. This is due to the conversion ratios in the driveline. See [13] or [11] for a more detailed description of driveline modeling.

LINKÖPING UNIVERSITY
ELECTRONIC PRESS

Copyright

Svenska

Detta dokument hålls tillgängligt på Internet - eller dess framtida ersättare - under en längre tid från publiceringsdatum under förutsättning att inga extraordinära omständigheter uppstår.

Tillgång till dokumentet innebär tillstånd för var och en att läsa, ladda ner, skriva ut enstaka kopior för enskilt bruk och att använda det oförändrat för ickekommersiell forskning och för undervisning. Överföring av upphovsrätten vid en senare tidpunkt kan inte upphäva detta tillstånd. All annan användning av dokumentet kräver upphovsmannens medgivande. För att garantera äktheten, säkerheten och tillgängligheten finns det lösningar av teknisk och administrativ art.

Upphovsmannens ideella rätt innefattar rätt att bli nämnd som upphovsman i den omfattning som god sed kräver vid användning av dokumentet på ovan beskrivna sätt samt skydd mot att dokumentet ändras eller presenteras i sådan form eller i sådant sammanhang som är kränkande för upphovsmannens litterära eller konstnärliga anseende eller egenart.

För ytterligare information om Linköping University Electronic Press se förlagets hemsida: `http://www.ep.liu.se/`

English

The publishers will keep this document online on the Internet - or its possible replacement - for a considerable time from the date of publication barring exceptional circumstances.

The online availability of the document implies a permanent permission for anyone to read, to download, to print out single copies for your own use and to use it unchanged for any non-commercial research and educational purpose. Subsequent transfers of copyright cannot revoke this permission. All other uses of the document are conditional on the consent of the copyright owner. The publisher has taken technical and administrative measures to assure authenticity, security and accessibility.

According to intellectual property law the author has the right to be mentioned when his/her work is accessed as described above and to be protected against infringement.

For additional information about the Linköping University Electronic Press and its procedures for publication and for assurance of document integrity, please refer to its WWW home page: `http://www.ep.liu.se/`

© Magnus Nilsson
Linköping, 30th March 2004